1-1-2005

Redesigning a compressor inlet guide vane for 0 to 60 degree stagger angles

Stephanie Waters
Ryerson University

Redesigning a Compressor Inlet Guide Vane for 0 to 60 Degree Stagger Angles

by

Stephanie Waters, B.Eng., McGill University, 2002

A project
presented to Ryerson University
in partial fulfillment of the
requirements for the degree of
Master of Engineering
in the Program of
Mechanical Engineering

Toronto, Ontario, Canada, 2005

Author's Declaration

I hereby declare that I am the sole author of this thesis or dissertation.

I authorize Ryerson University to lend this thesis or dissertation to other institutions or individuals for the purpose of scholarly research.

I further authorize Ryerson University to reproduce this thesis or dissertation by photocopying or by other means, in total or in part, at the request of other institutions or individuals for the purpose of scholarly research.

Abstract

This report's objective is to reduce the total pressure loss coefficient of an inlet guide vane (IGV) at high stagger angles and to therefore reduce the overall fuel consumption of an aircraft engine. IGVs are usually optimized for cruise where the stagger angle is approximately 0 degrees. To reduce losses, four different methodologies were tested: increasing the leading edge radius, increasing the camber, creating a "drooped" nose, and creating an "S" curvature distribution. A baseline IGV was chosen and modified using these methodologies to create 10 new IGV designs. CFX was used to perform a CFD analysis on all 11 IGV designs at 5 stagger angles from 0 to 60 degrees. Typical missions were analyzed and it was discovered that the new designs decreased the fuel consumption of the engine. The IGV with the "S" curvature and thicker leading edge was the best and decreased the fuel consumption by 0.24%.

Acknowledgements

I would like to thank Professor Alighanbari for his guidance on this project. Special thanks goes to the Compressor Aerodynamics group at Pratt & Whitney Canada, especially to Gary Weir and Doug Roberts who generously gave so much of their time to teach me so much and to answer all of my questions. Finally, I would like to thank Eric Benner for his help in proof reading but more importantly for his support.

Table Of Contents

List of Tables

List of Figures

Nomenclature

a: Angle of attack

A_{geo}: Geometric area

A_{aero}: Effective aerodynamic area

BF: Blockage factor

c: Blade chord

C_D: Discharge coefficient

C_m: Velocity in the meridional direction (stationary frame)

C_u: Velocity in the tangential direction (stationary frame)

C_x: Velocity in the axial direction (stationary frame)

FC: Fuel consumption

M: Mach number

P_S: Static pressure

P_T: Total pressure

T_T: Total temperature

r: Nose radius

RPM: Rotations per minute

U: Blade speed

V_m: Velocity in the meridional direction (rotating frame)

V_u: Velocity in the tangential direction (rotating frame)

V_x: Velocity in the axial direction (rotating frame)

W: Mass flow

WTAPact: Actual mass flow based on temperature, area, and pressure

WTAPideal: Ideal mass flow based on temperature, area, and pressure

α: Flow angle (stationary frame)

β: Flow angle (rotating frame)

γ: Ratio of specific heat capacities

δ: Deviation

η: Efficiency

ξ: IGV stagger angle

φ: Flow inclination angle

χ: Blade angle

ω: Loss coefficient

Subscript 1: At IGV inlet or blade leading edge

Subscript 2: At IGV exit or blade trailing edge

Subscript 3: At compressor exit

1.0 - Introduction

1.1 - Project Motivation

Variable inlet guide vanes in a compressor, known as IGVs, are used to improve the matching of airflow to geometry at lower compressor speeds. The compressor spends most of its time at cruise where the IGVs are at 0 degree stagger. Therefore, IGVs are generally designed to minimize loss at zero degree stagger angle. The stagger angle, ξ, is defined as the angle of chord line measured from the axial direction [1]. The definition of total pressure loss coefficient, ω, is given below [2]. This is commonly referred to as "loss" throughout this project. P_T refers to total pressure and P_S refers to static pressure. Subscript one indicates that it is at the inlet and subscript two indicates that it is at the exit.

$$\omega = \frac{P_{T1} - P_{T2}}{P_{T1} - P_{S1}}$$

However, the IGVs can spend a not insignificant amount of time at off-design conditions where they can experience stagger angles ranging up to 60 degrees closed. The higher stagger angles generally occur during part-power settings such as taxiing, loitering, and landing. For longer missions, the time spent at cruise tends to be a high percentage of the mission as a whole. Thus, it is reasonable to design the engine so that it is optimal at the cruise condition. For an IGV, this means designing the IGV for 0 degree stagger.

For shorter missions, the time spent at cruise is often a small percentage of the mission as a whole. The airplane could finish climbing and then have to start the descent a few minutes later. For missions such as this, the engine, and thus the IGVs, would spend the majority of their time operating at off-design conditions. In such cases, it is no longer sensible to optimize the IGV solely for 0 degree stagger. Ideally, the IGV would be redesigned so that it is also efficient at higher stagger angles as well. Realistically, to achieve better efficiencies at higher stagger angles, some efficiency at lower stagger angles would have to be sacrificed. The important overall parameter is the total fuel

burned for the mission. Thus, the important parameter for the IGV is its average efficiency, weighted for the time spent at each IGV setting. The goal of this project is to design a new IGV that offers reduced losses for higher stagger angles, and thus would have a lower total fuel consumption when the entire mission is considered.

1.2 - Background Theory

IGVs are part of an aircraft engine's compressor. Figure 1 shows a typical turbofan engine. Figure 2 shows a schematic of the compressor of typical turbofan engine designed by Pratt & Whitney Canada (P&WC); the IGV is located just upstream of the axial compressor. IGVs are airfoils similar to stators except that they can rotate around a specified stacking axis. The IGVs can be rotated to a specific stagger angle in order to change its incidence with the airflow. It should be noted that there is a key distinction between an inlet guide vane airfoil and all of the other compressor stators. While compressor stators decelerate, and thus diffuse the flow, IGVs actually serve to accelerate the flow. In fact, the compressor IGV is more similar in nature to a turbine blade than to a compressor stator.

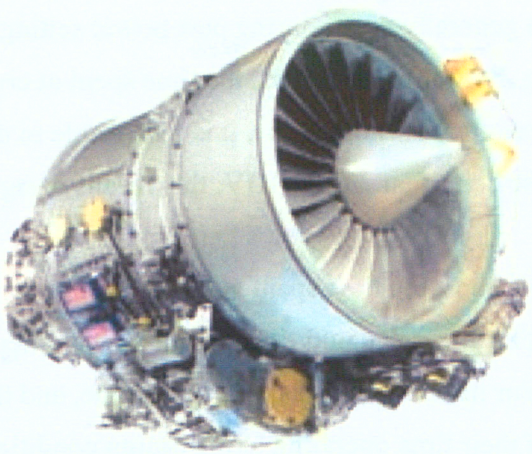

Figure 1 - P&WC turbofan engine [3]

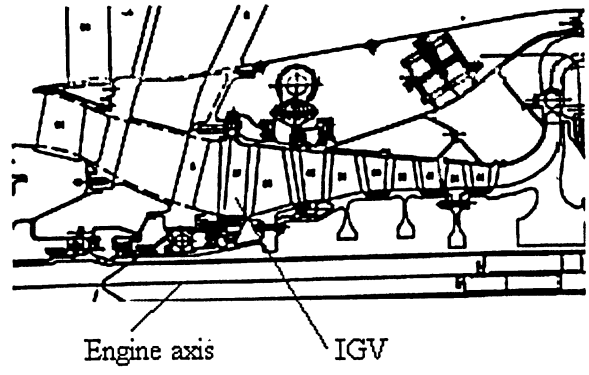

Figure 2 - Compressor schematic

The compressor design is typically optimized for cruise conditions and the flow path geometry is designed for those specific conditions. When other engine thrusts are required and the mass flow requirement is reduced, the flow path geometry is no longer ideal. The IGVs primary purpose is to modify the airflow direction so that it matches the geometry of the blades for off-design conditions.

Ideally, it would be desirable to vary the angles of each blade row and also adjust the height of the flow path in order to optimize the geometry for each engine condition. This is infeasible though, as it would drastically increase the complexity of the compressor. A common compromise is to have one or more rows of variable stators, including IGVs upstream of the compressor that are adjustable.

A rotor can be complex to analyze because it is rotating and can be examined in either a stationary or rotating frame. Figure 3 shows a diagram of the rotor in the stationary frame. In this case, a velocity triangle can be drawn that would greatly simplify the problem. Figure 4 shows a velocity triangle for a rotor in the rotating frame. U is the blade speed of the rotating rotor. V is the velocity of the flow while V_x is the flow velocity in the axial direction, both in the rotating frame. Alpha is the flow incidence angle of the rotor in the stationary frame. In this case, alpha is zero, which means that the airflow is hitting the rotor head-on. Beta is the flow incidence angle of the rotor in the rotating frame. Since the blade is rotating, beta will not equal zero even though alpha does.

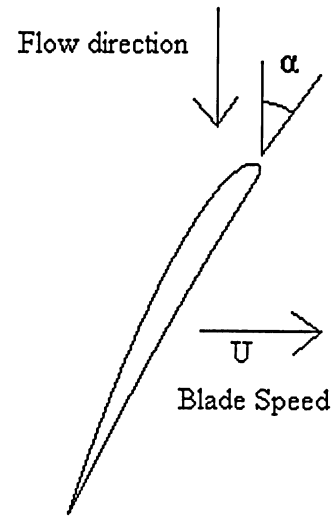

Figure 3 - Rotor diagram in the stationary frame

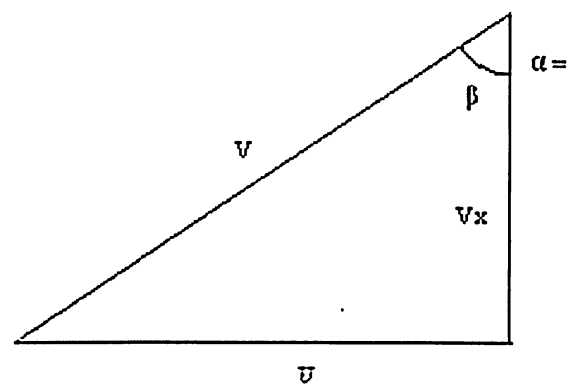

Figure 4 - Rotor velocity triangle, alpha zero

Figure 5 shows a rotor velocity triangle for a case where alpha is not zero. This means that in the stationary frame, the airflow hits the rotor at some angle. C is the flow velocity in the stationary frame where C_x is its component in the axial direction and C_u is its component in the tangential direction. V_u is the flow velocity in the tangential direction in the rotating frame. C_u and V_u add up to equal U, the blade speed.

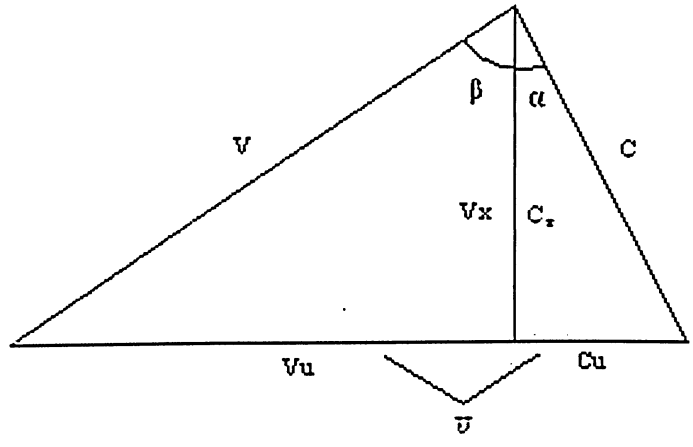

Figure 5 - Rotor velocity triangle, alpha non-zero

The engine is required to produce low thrust for off-design conditions such as taxiing. The engine RPM, as well as the pressure ratio and mass flow, are considerably lower for such part-speed conditions, as compared to design point. The difficulty arises when the blade speed is lowered. For example, if the blade speed is reduced by half, the axial velocity of the flow reduces to a value less than half of the design point axial velocity. The problem becomes apparent when velocity triangles are drawn for a first-stage rotor in this situation, as seen in Figure 6. Subscript one indicates it is for the design speed condition and subscript two indicates it is for the part speed condition. If the ratio of axial velocity to blade speed decreases then the air angle, β, increases. If the blade rows can only be only optimized for one angle, then the compressor would then become mismatched for the part-speed conditions.

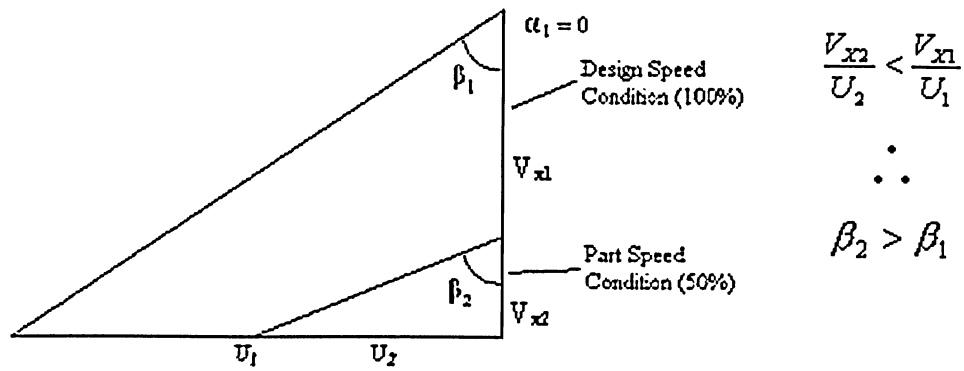

Figure 6 - Velocity triangles comparing design speed to 50% speed conditions

The IGV turns the flow and thus changes the incidence angle of the first blade row. If the IGVs were positioned correctly, then the IGVs could turn the flow by α so that the incidence angle of the first blade row would be the same as it was at the design point, as seen in Figure 7. Ideally, IGVs would precede each blade row and adjust the flow as necessary but that would be too complicated, bulky, and very costly.

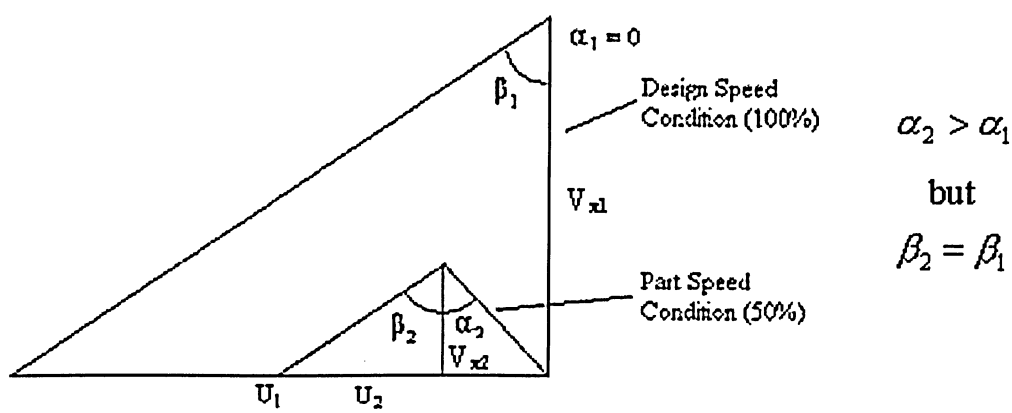

Figure 7 - Velocity triangles at compressor rotor entry showing the effect of an IGV

A second benefit of IGVs is that they can decrease the amount of work done on the flow for a given speed. This means that to maintain the same thrust, the engine has to run at higher speeds. Therefore, the engine can still run at relatively high speeds, even

when it is producing low thrust. If the engine is required to produce more thrust, then it can do so more quickly since the RPM is already fairly high and significantly less acceleration of the spool is required.

IGVs are not the only options for solving compressor mismatching. Often the first row of stators has some element of variable geometry as well. Air is also commonly bled off at points throughout the compressor in order to try to match the airflow angles with the blading.

1.3 - Literature Review

During the research for this project, no papers were found on the optimization of compressor IGVs for a large range of stagger angles. However, research done on conventional airfoils in general would be applicable to this problem, as the principles would be very similar. Unfortunately, the majority of papers on airfoil optimization involved using an inverse design method where an objective pressure profile was chosen, and a computer model would create the optimum blade shape [4]. It was not the intent of this project to experiment with inverse design codes so these papers were not very useful.

Sanz et. al. [5] explored numerous guide vane shapes that were designed to operate with high efficiency over a 60 degree inlet flow angle range. These guide vanes were intended for a wind tunnel but the theories discussed can be applied to a compressor as well. Sanz used an inverse design code to create the IGV designs and then tested them in a wind tunnel. His results and conclusions were very useful in determining a starting point for this project. Specifically, several IGV designs in this project were based on the Lewis number 3 design from Sanz's paper.

Tuck [6] discovered the relation between angle of attack, chord, and nose radius such that leading edge separation would not occur. The angle of attack has to be greater than the term on the right side of the equation in order for the flow to not have leading edge separation. The equation is shown below. Angle of attack is represented by a, chord by c, and nose radius by r.

$$a > 0.818(r/c)^{1/2}$$

From his work, it can be seen that airfoils with larger leading edge radius can go to higher angles of attack without the leading edge flow separating. This idea was fundamental in the design of many of the new IGVs.

Tuck wrote another paper [7], this time in collaboration with A. Dostovalova, concerning "drooped" nose airfoils and how they can delay leading edge separation. They discovered the relation below for this type of airfoil.

$$a > 0.912(r/c)^{1/2}$$

A "drooped" nose is where much of the camber is concentrated in the front tip of the airfoil and the leading edge is effectively more "closed" locally than the rest of the blade. Several IGV designs were created while experimenting with this concept.

1.4 - Project Approach

An IGV from a turbofan engine was chosen as a baseline. This engine is designed for short to medium range flights. This IGV has a small leading edge radius and is only slightly cambered. There is some twist in the airfoil so that the blade turns the flow differently at the shroud than at the hub. In the 0 stagger condition, the blade is designed to increase rotor pre-swirl at the tip, while reducing it at the hub. This is to reduce the relative Mach number at the tip of the following rotor. However, the average amount of overall turning is close to zero.

From the baseline case, ten new IGV designs were created. Each design, including the baseline case, was analyzed at the following five stagger angles: 0, 15, 30, 45, and 60 degrees. The new IGVs were designed by exploring four different ideas on how to reduce the overall losses, but more specifically, to reduce losses at high stagger angles.

The four different ideas were varied but were all based on the idea of reducing the losses at high stagger angles. The first involved increasing the leading edge radius of the airfoil as well as increasing the maximum thickness. The second concerned increasing the

camber uniformly throughout the blade. The third involved increasing the camber in the front tip of the airfoil to create a "drooped" nose. The last theory concerned changing the curvature distribution of the blade so that an "S" shape was achieved like that of the Lewis number 3 design from Sanz's paper.

1.5 - Project Mission

An IGV is typically designed for one set of conditions. The goal of this paper is to discover methods to improve the IGVs at higher stagger angles such that the overall mission efficiency of the engine is improved. If such methods are discovered, then it is hoped that with further testing a more efficient IGV, and thus engine, could be developed.

2.0 - Computational Fluid Dynamics (CFD)

2.1 - Why CFD

CFD is a powerful tool that makes it possible to analyze a myriad of different fluid dynamic models with relative ease. It does this by dividing the area being analyzed into many small control volumes. The Navier-Stokes equations are then applied to each control volume, relating such variables as pressure and temperature, among others, with the neighboring control volume's variables [8]. The entire system is then solved numerically. The final result is a comprehensive solution of the fluid flow.

CFD is currently the dominant method of analyzing fluid flow problems, as it is a quick, powerful and convenient tool [9]. However, it does have its share of weaknesses. CFD does a good job of accurately describing laminar flow. However, it can have difficulty accurately describing turbulent flow, which can be much harder to model. Models can sometimes be wrong due to incorrect assumptions on the part of the user.

More accurate and realistic results would be gained from physical testing but, due to its cost and difficulty, it is infeasible for a project such as this because it is not simply a matter of testing a known design. CFD was used to evaluate many alternative designs and helped to narrow down the most promising design alternatives for future experimental work.

2.2 - Why CFX

CFX was chosen as the CFD software for this project for many reasons. It is a powerful and user-friendly software that is particularly suited for this type of project because it has many features specifically designed for turbo machinery. This greatly simplified model setup and saved a lot of time. For this project, the CFX version 5.6 solver, along with "pre" and "post" modules, were used.

CFX-Turbogrid was the meshing software used; it was also designed with several turbo machinery functionalities that make the whole process easier. Turbogrid generated the mesh that was then exported to CFX Pre where the problem was setup and defined. The CFX Solver was used on a computer cluster of 2-3 nodes working in parallel to solve each case. Finally, the results were examined and calculated in CFX Post.

3.0 - Model Setup

3.1 - Problem Simplification

To determine the overall change in fuel consumption, it was necessary to examine the engine's missions to determine how long the IGV spends at each angle and mass flow. The IGV changes stagger angle frequently throughout the mission with angles ranging from 0 and 60. To make the problem manageable, only five stagger angles were analyzed for each IGV design.

Initially, it was thought to keep the mass flow constant throughout all stagger angles so that all of the models would be directly comparable. This proved to be problematic, as the flow would choke at the higher stagger angles due to the reduced flow area. In reality, the mass flow in the engine does decrease as the IGV stagger increases, so no actual choking should occur in the engine. Therefore, it was decided that the mass flow for each stagger angle would mimic the operating conditions of the engine in order to achieve more realistic results. Thus, a mass flow was assigned to each blade stagger angle. This is a minor simplification as the mass flow is not constant for each stagger angle. There is a small amount of variation depending on the exact running conditions. For this project, however, this variation was deemed small enough to be ignored. In addition, all loss values are normalized by dynamic head, so exact engine mass flows are not crucial.

It was decided that the best approach to this problem was to select representative running conditions. Typical running conditions for taxiing, take-off, climbing, cruising and landing were chosen. For example, there may be three running conditions for climb that, in terms of IGV position and conditions, are very similar. To simplify the problem, the most typical one of the three was chosen to be the representative running condition. The times spent at the two omitted conditions were included with the time of the representative running condition. In this way, a mission which may have over 20 running conditions can be simplified to down to 5 representative running conditions.

Linear interpolation was necessary because the CFX models were evaluated only for 5 predefined angles that invariably would not match the IGV angles of the 5 representative running conditions.

3.2 - Model Specifications

In general, the default settings in CFX Pre were used for all of the models. The High-Resolution Advection scheme was used since it tends to produce very accurate results. The scheme that is used in CFX is based on work done by Barth and Jesperson [10].

For turbulence modeling, the Shear Stress Transport (SST) model was used because it is well suited to handle flow separation over curved surfaces [11]. The k-ε model was avoided because it generally under-estimates the impact of leading edge separation. A comparison was made by Roberts and Steed [12] between the k-ε and the SST turbulence models for a centrifugal compressor. The results were compared to experimental data and it was shown that the SST model did indeed produce much better results. For these reasons, it was decided that the SST model would be ideal.

Each mesh domain for a given case consisted of 5 boundary families: inlet, exit, wall, and 2 periodic sides. These boundaries can be seen in Figure 8. The flow was modeled assuming a steady-state, compressible, fully turbulent flow.

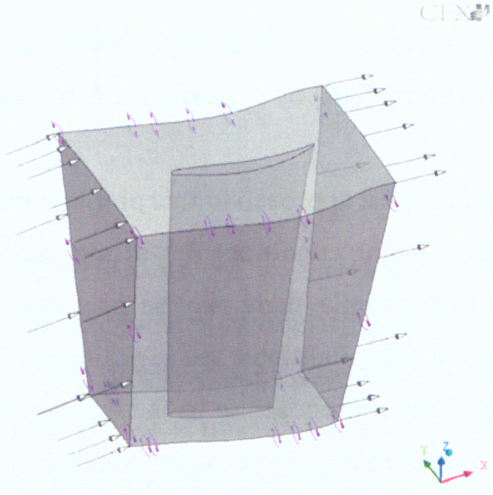

Figure 8 - Control volume for IGV10

Data for the boundary conditions of the inlet was fortunately available. The total pressure, total temperature, phi angle, and alpha angle profiles were used to define the

inlet boundary condition. Phi is the inclination angle with respect to the meridional and is shown in Figure 9. Alpha is the flow angle with respect to the meridional and is shown in Figure 10. The boundary condition profiles are plotted in Figure 11 to Figure 15. It was assumed that there would be moderate turbulence at the inlet so the inlet turbulence boundary condition was set to medium (intensity = 5%) [13]. This is standard practice at P&WC.

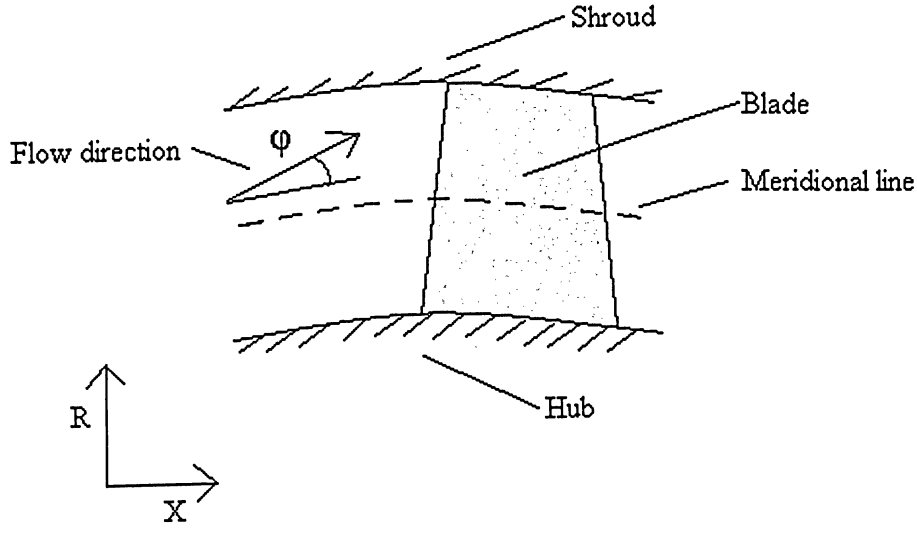

Figure 9 - Flow path showing phi

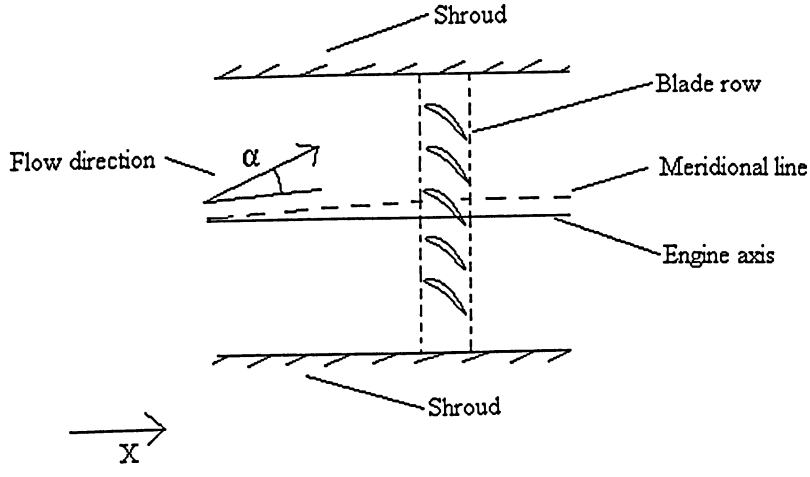

Figure 10 - Flow path (bird's eye view of previous figure) showing alpha

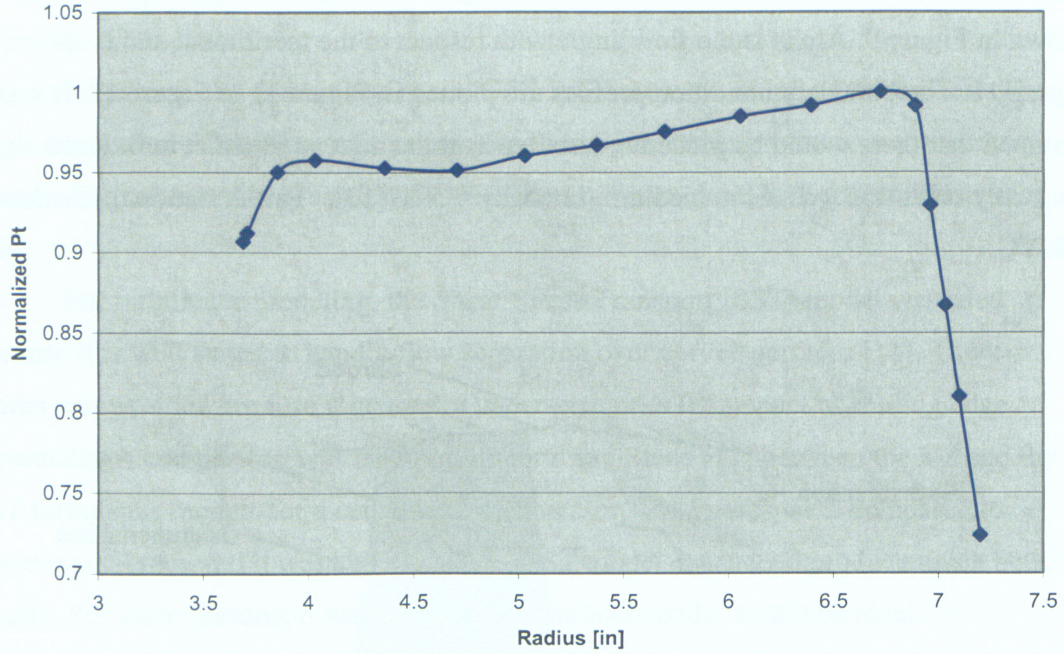

Figure 11 - Boundary condition profile - normalized inlet total pressure

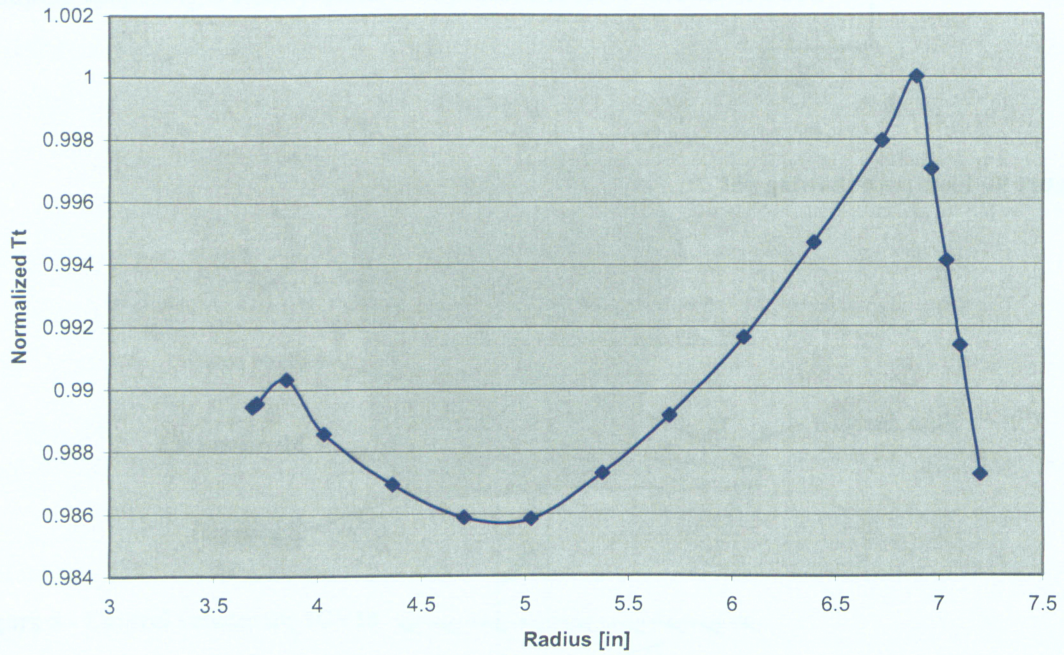

Figure 12 - Boundary condition profile - normalized inlet total temperature

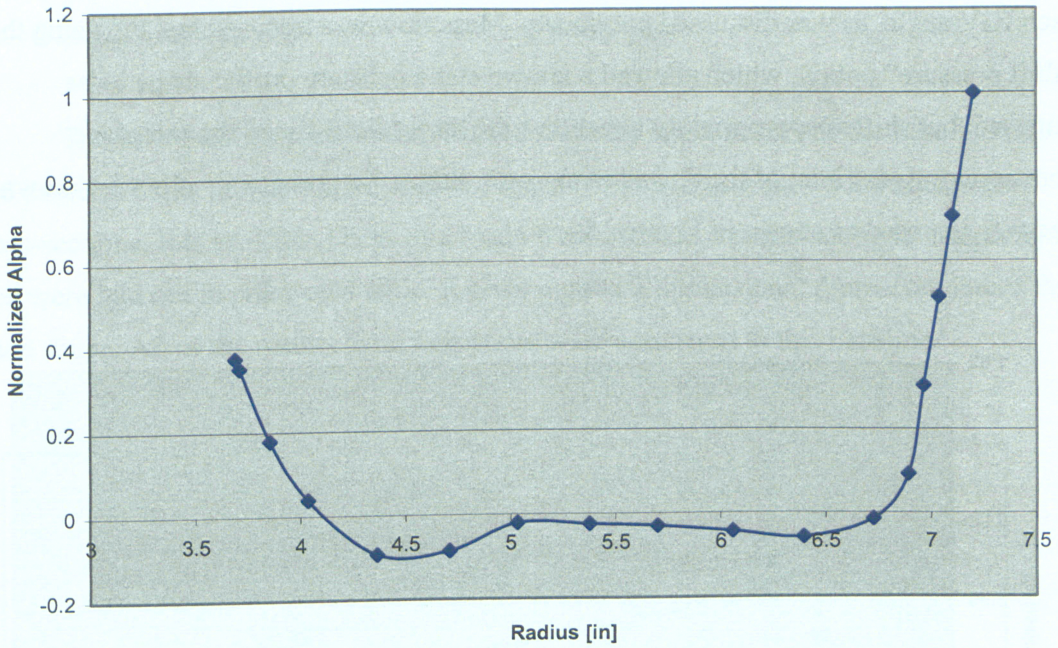

Figure 13 - Boundary condition profile - normalized inlet flow angle

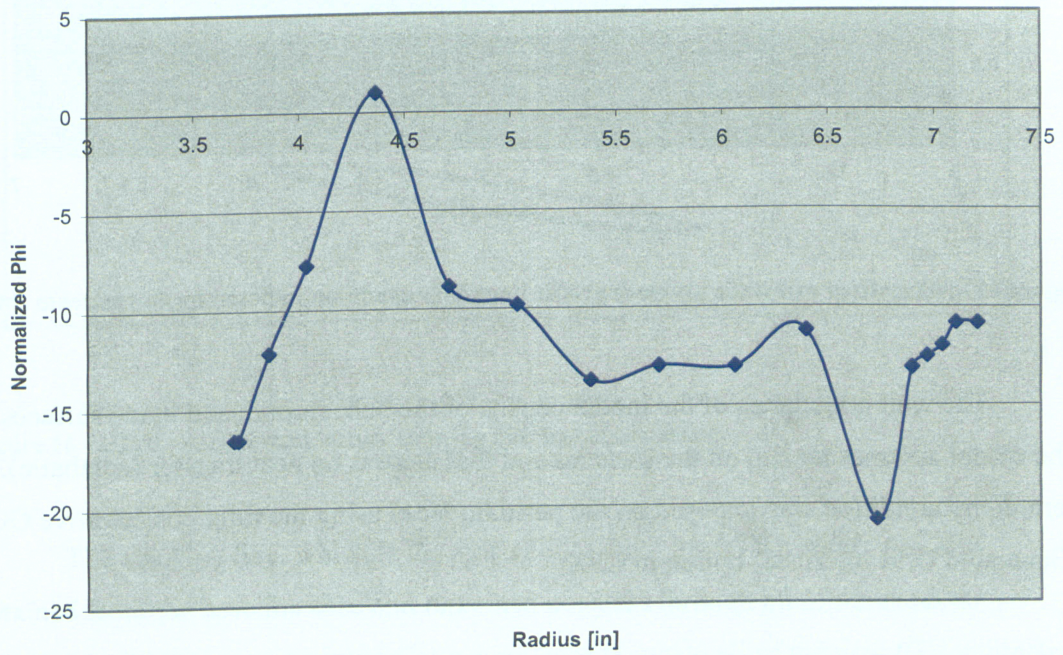

Figure 14 - Boundary condition profile - normalized inlet flow inclination angle

At the exit boundary condition, the mass flow rate was set to a particular value for each IGV angle, as was discussed previously. Mass flow was imposed in CFX using the "shift pressure" option, which allowed a known static pressure profile shape to be imposed, but shifted appropriately to achieve the target flow. Since the exit plane corresponds to the inlet of the downstream rotor, this static pressure profile was known, and was imposed as shown in Figure 15.

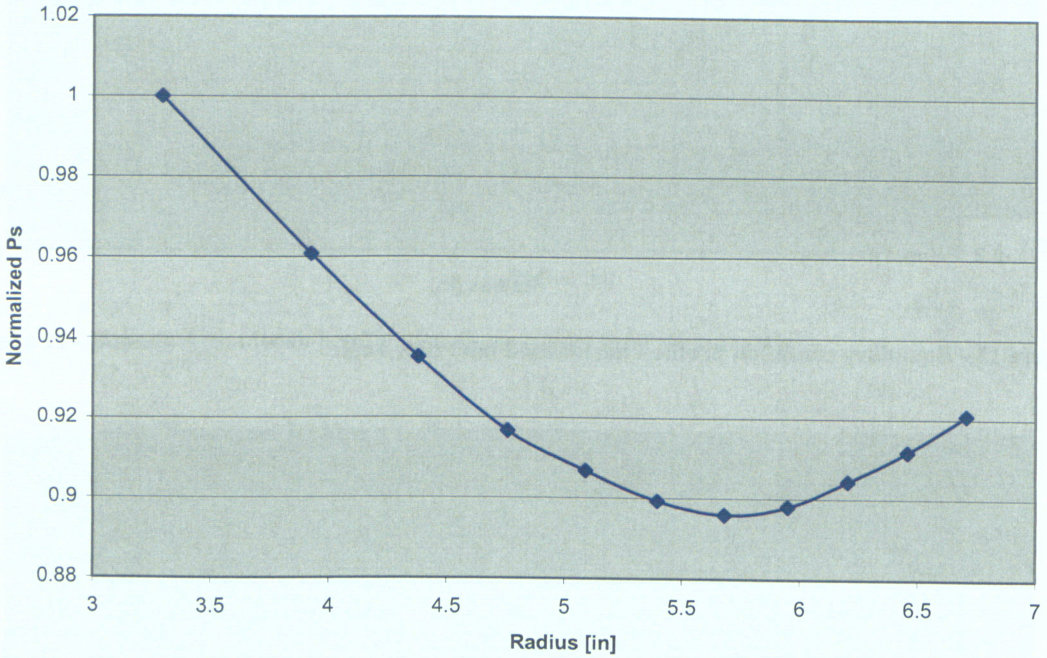

Figure 15 - Normalized exit static pressure profile boundary condition imposed by downstream rotor

The wall boundaries of the model consist of the hub, shroud, and blade surfaces. The model assumes no slip on the surfaces and that there is no heat transfer (adiabatic). A periodicity condition was imposed on the periodic faces using the fully conservative GGI (Generated Grid Interface) option in CFX.

4.0 - Geometry Creation

4.1 - General Methodology

The flow path geometry was obtained from the same engine as the baseline IGV. The baseline blade profile can be seen in Figure 16. This figure shows the blade in six cross-sections. It is as if thin slices of a blade were taken at 6 points along its length and then were laid out in order on a table. It gives a good 2 dimensional representation of the blade shape. All of the results from new IGVs were compared to this baseline.

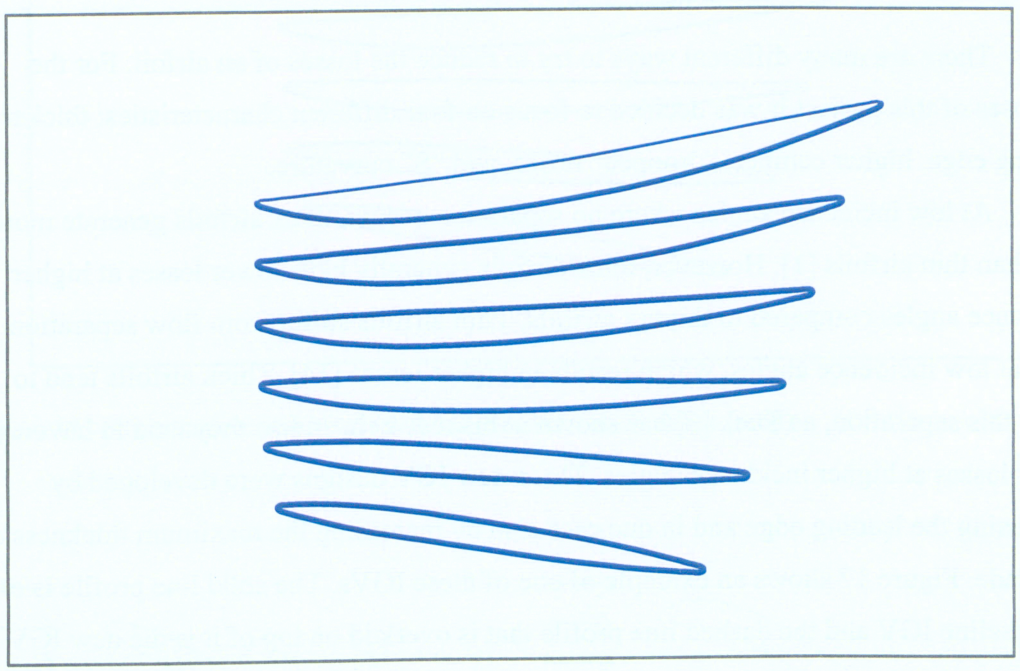

Figure 16 - IGV0 - Airfoil section cuts showing baseline blade shape

The stacking line, which is the axis about which the IGV rotates, was also obtained from the baseline case and remained constant through all of the models. Proprietary P&WC programs and Catia were used to create all of the new IGV geometry files.

The intent of this project was not to redesign the entire IGV, but to test various ideas on reducing losses, specifically for higher incidences. When modifying the baseline IGV, efforts were made to change one variable at a time. That way, changes in the results could be attributed to the modification of that one variable. It was, however, not always possible to isolate the change to one variable. Other variables often needed to be varied as well in order to maintain a sensible airfoil shape. These extra changes were minimized as much as possible but were unavoidable.

4.2 - Design Modifications

There are many different ways to try to reduce the losses of an airfoil. For the purposes of this project it was decided to focus on four different characteristics: thicker leading edge, higher camber, "drooped" noses, and "S" curvature.

At low incidence angles where no separation occurs, thick airfoils generate more loss than thin airfoils [1]. However, thick airfoils generally have lower losses at higher incidence angles compared to thinner airfoils. Thin airfoils suffer from flow separation even at low incidence angles, which results in higher losses [14]. Thick airfoils tend to delay this separation, as Tuck [6] has shown in his research, and so they tend to have lower losses at higher incidence angles. Three new IGV designs were developed by thickening the leading edge and in one case also by increasing the maximum thickness of the blade. Figure 17 shows an example of one of these IGVs. The solid line profile is of the baseline IGV and the dashed line profile that is overlaid on top of it is the new IGV design.

Modifying the camber of the blade is another possible method of decreasing the losses at higher stagger angles. By increasing the camber angle in the front of the airfoil, it is possible to reduce the effective incidence angle at high IGV angles. At zero degrees, the airfoil would essentially be at a small negative incidence. This has the effect of shifting the loss bucket so that the airfoil would tend to have lower losses at a higher angle. This is demonstrated in Figure 18, where it can be seen how curving the front section of the blade lets the airfoil meet the incoming airflow at a reduced angle. By

varying the inlet blade angle of the blade as well as the curvature, two new IGV shapes were created. One of them can be seen in Figure 19.

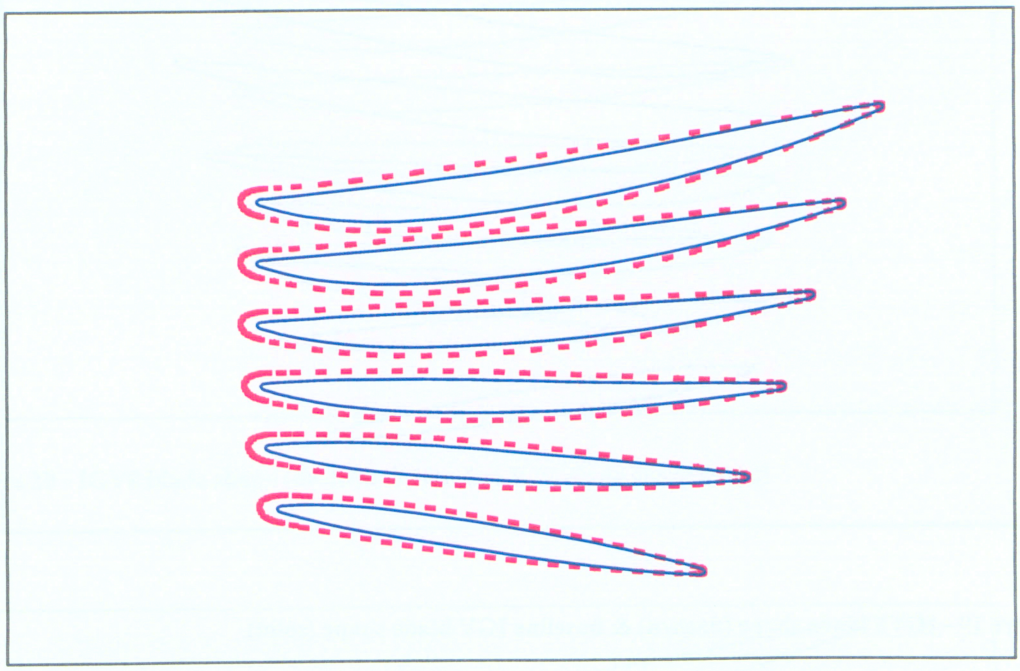

Figure 17 - IGV3 blade shape (dashed) & baseline IGV blade shape (solid)

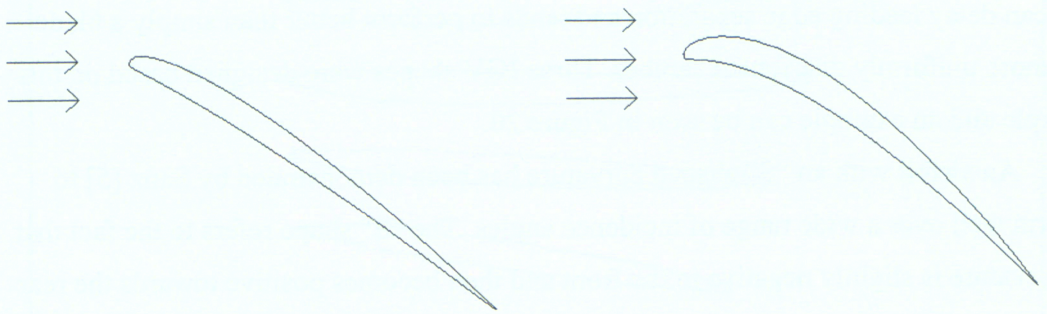

Figure 18 - Original blade vs. blade with increased camber in front section

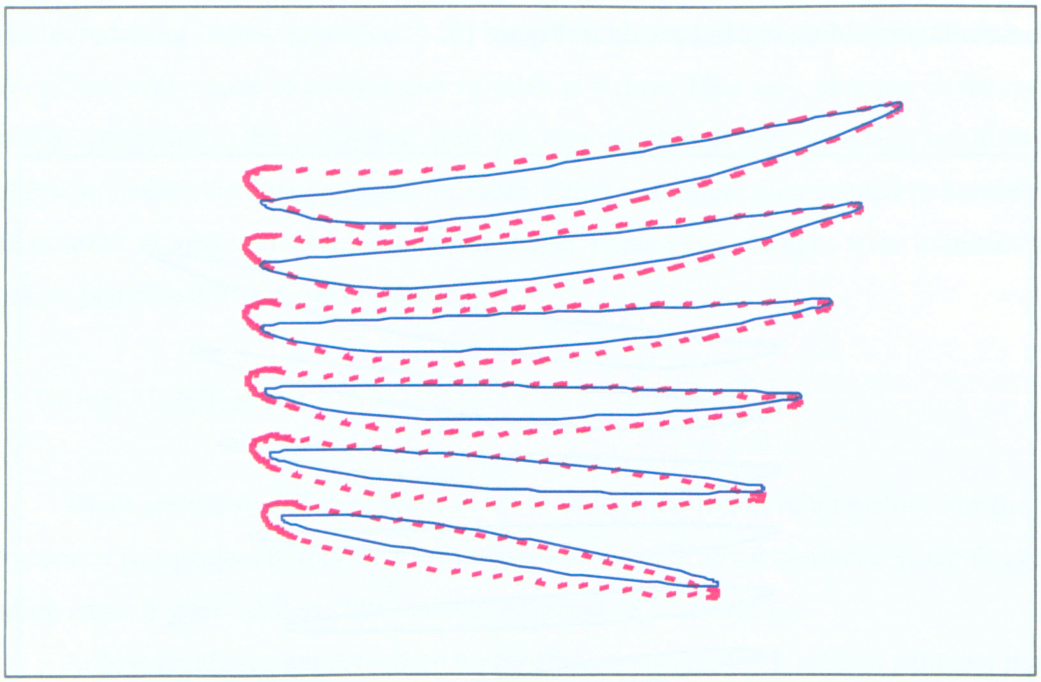

Figure 19 - IGV5 blade shape (dashed) & baseline IGV blade shape (solid)

An airfoil with a drooped nose works on the same principal as the previous camber method. However, in this case the curvature in the blade is concentrated in the front tip of the blade. Research by Tuck & Dostovalova [7] has shown that a drooped nose can delay leading edge separation and tends to perform better than simply a blade with more uniformly distributed camber. Three IGV shapes were designed based on this principle and an example can be seen in Figure 20.

An airfoil with an "S" shaped curvature has been demonstrated by Sanz [5] to perform well over a wide range of incidence angles. The "S" shape refers to the fact that the curvature is slightly negative in the front and then becomes positive towards the rear of the blade. Two final IGV designs were created based on this "S" shape, one seen in Figure 21.

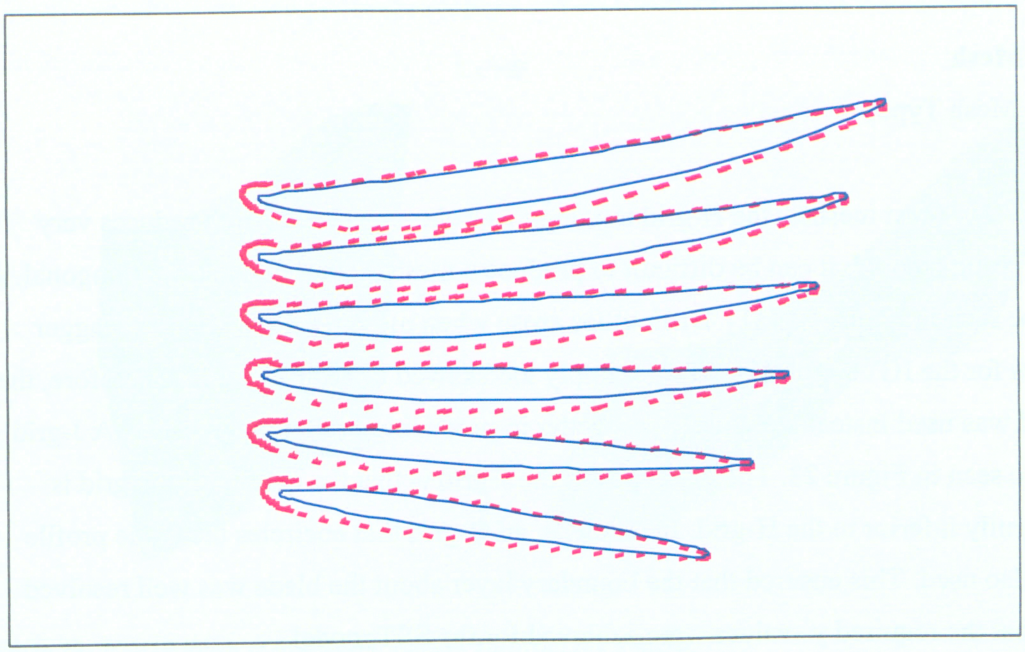

Figure 20 - IGV8 blade shape (dashed) & baseline IGV blade shape (solid)

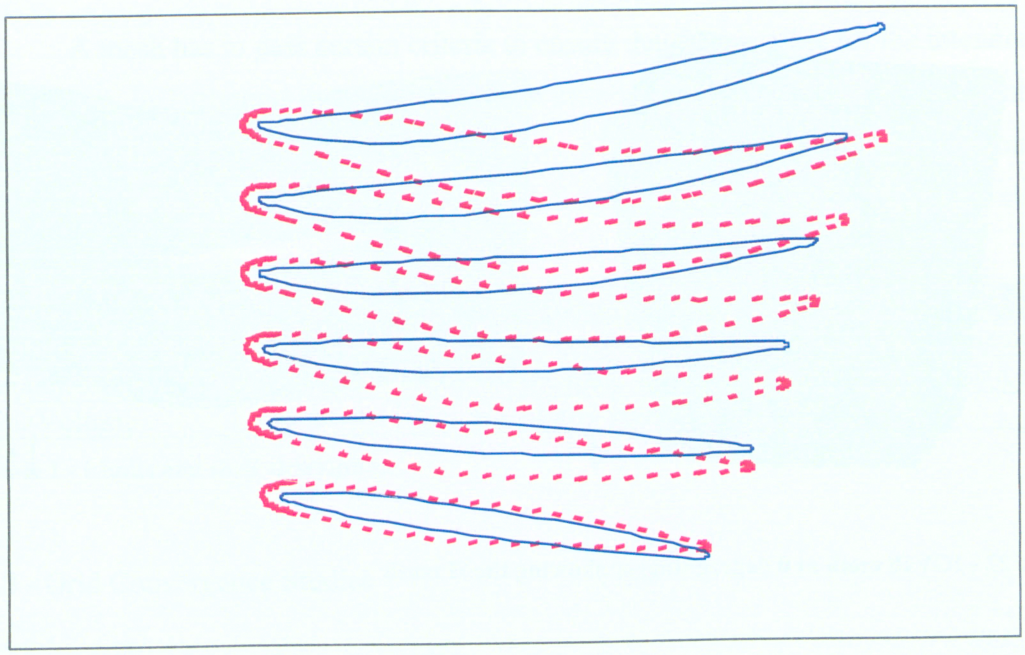

Figure 21 - IGV10 blade shape (dashed) & baseline IGV blade shape (solid)

5.0 - Mesh

5.1 – Mesh Type

For most meshes, the H-grid topology was chosen. The H-grid produces very good results though it can be difficult to produce a mesh that is reasonably orthogonal, as can be seen in Figure 22 [11]. Difficulties arose when meshing the 60-degree stagger angles for the IGVs. The H-grid was simply too skewed to be acceptable. Therefore, the J-grid was used instead because it was better in producing orthogonal meshes. A J-grid can be seen in Figure 23. The drawback to the J-grid is that the quality of the grid is inherently inferior to the H-grid. In all cases, an O-grid that encircles the blade profile was also used. This ensured that the boundary layer about the blade was well resolved and that the required y^+ values were achieved for the SST model.

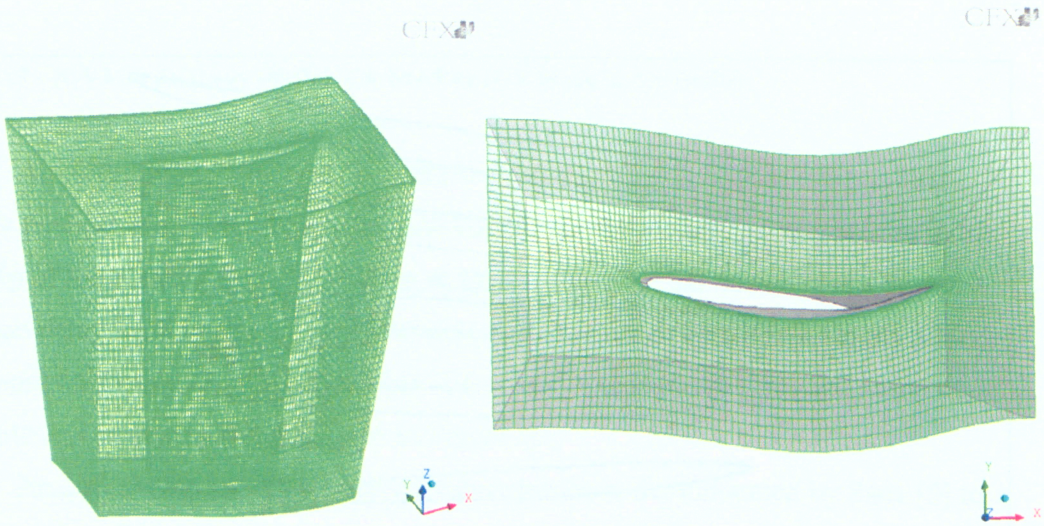

Figure 22 - IGV10 mesh at 0 degree stagger showing the H mesh

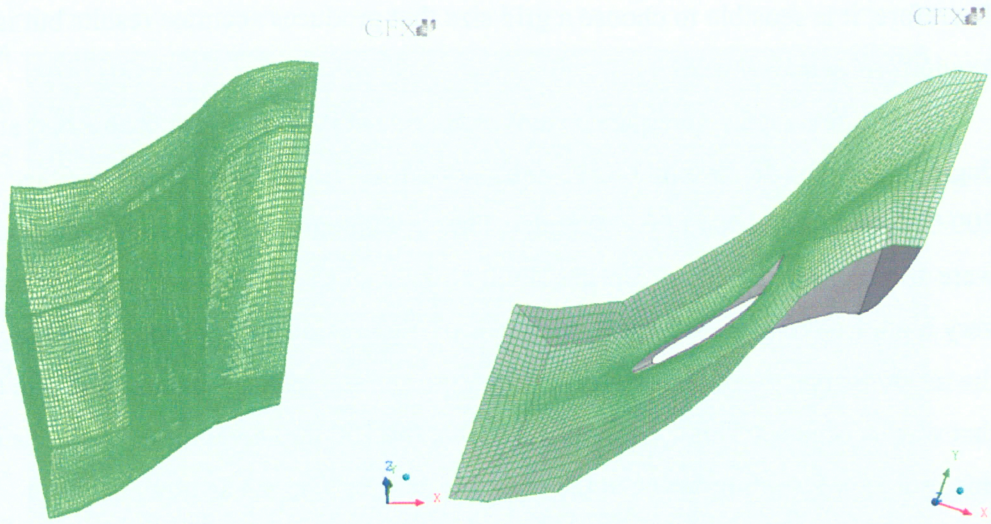

Figure 23- IGV10 mesh at 60-degree stagger showing the J mesh

5.2 - Mesh Quality

A mesh has to pass certain criteria to ensure that it is suitable for the intended application. In Turbogrid there are three main criteria: minimum face angle, element volume ratio, and minimum volume. Limits can be set for each of these criteria. These limits are summarized in Table 1. The default limits were kept for all these criterions.

Limit Name	Limit	Description
Min. Face Angle	min. 15	Min. angle between two adjacent faces, a measure of skew
Element Vol. Ratio	max. 100	Ratio of the max. and min. volumes that touch a node
Min. Volume	min. 0	Volume of any volume touching a node

Table 1 - Limits and their descriptions

5.3 - Grid Convergence Studies

Two grid convergence studies were conducted to determine how fine the mesh needed to be to achieve good predictions, which were essentially independent of the mesh. Generally, the accuracy of the results improves as the mesh size grows larger. However, the larger the mesh is, the more time and computing power it requires.

Therefore, it is sensible to choose a grid size that produces accurate results but is not too unwieldy to work with.

The first grid convergence study was done at 0 degrees and the second at 60 degrees, both for the baseline IGV. Each examined four different grid densities: 100 000, 200 000, 500 000, and 1 000 000 nodes. For the 60 degree grid convergence study, there were convergence problems for the 100 000 node mesh and the residual error terms were very high. Looking more closely, the areas of high residuals were spaced out regularly at the mesh intersections. This suggested that the convergence problems were due to a mesh that was too coarse. This made it obvious that the 100 000 node mesh was not suitable for this problem. Deciding between the other mesh sizes was not as obvious.

Loss, being of primary importance to this project, was plotted versus grid size so its sensitivity could clearly be seen. This is plotted in Figure 24 and Figure 25. Table 2 shows how much the loss variable changes for every increase in mesh size, for both grid convergence studies. It can be seen that there is a sizeable change in loss when the grid is increased from 100 000 to 200 000, as well as when the grid is increase from 200 000 to 500 000. There is less of a 2% difference in the loss results when the grid size is increased from 500 000 to 1 000 000. However, the pressure ratio is used to calculate efficiency, not loss. If the pressure ratio or efficiency itself were examined in Table 2, then it could be seen that there is less than a 0.05% difference between the 500 000 to 1 000 000 meshes. Therefore, it was decided that the 500 000 element mesh would suitable for this project.

Mesh Sizes	Change in Loss		Change in Pressure Ratio		Change in Efficiency	
(in thousand)	0 Degree	60 Degree	0 Degree	60 Degree	0 Degree	60 Degree
100-200	22.090%	13.232%	-0.281%	-1.061%	-0.153%	-1.365%
200-500	15.154%	3.095%	-0.131%	-0.081%	-0.072%	-0.103%
500-1000	-1.768%	1.669%	0.007%	-0.027%	0.004%	-0.034%

Table 2 - Grid sensitivity

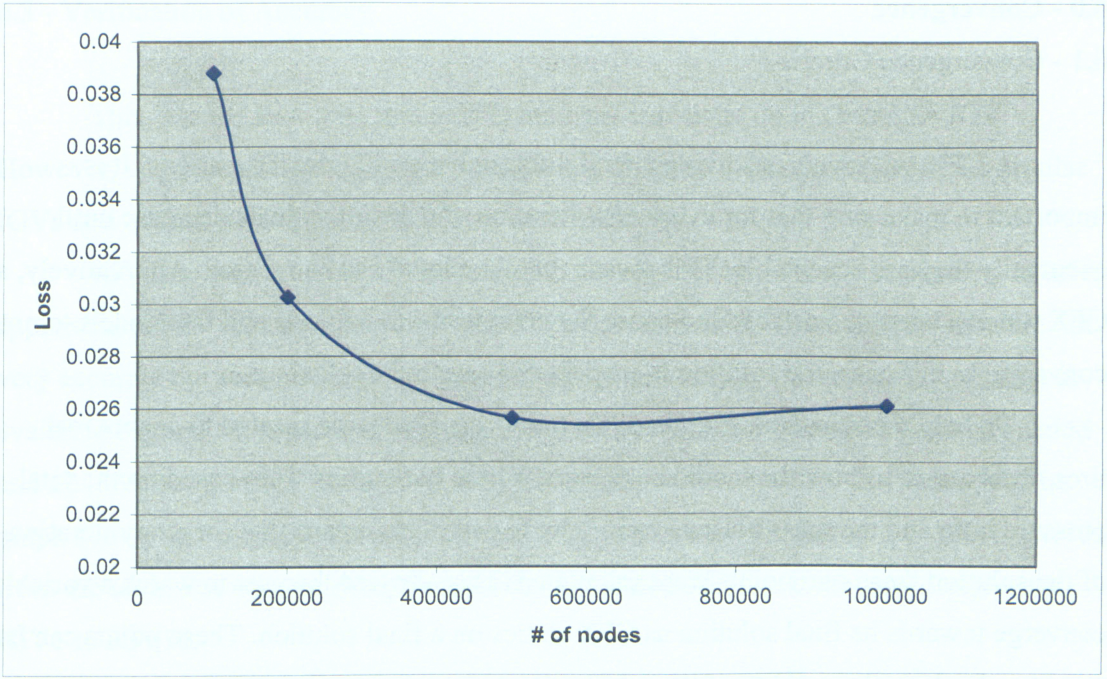

Figure 24 - Predicted loss vs. grid size at 0 degrees stagger

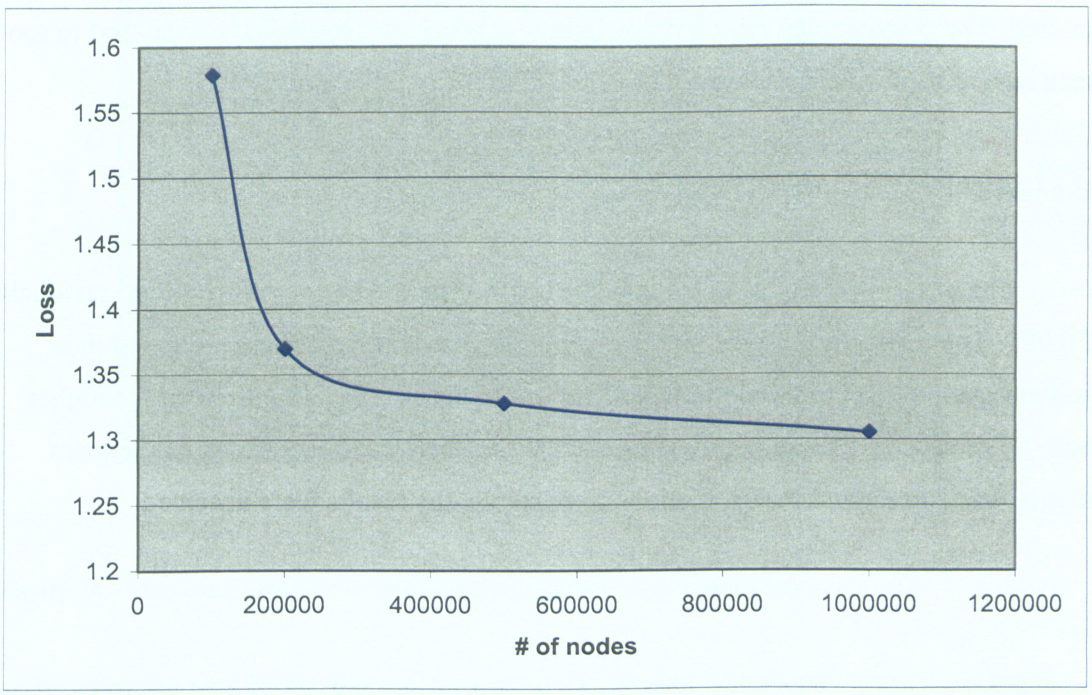

Figure 25 - Predicted loss vs. grid size at 60 degrees stagger

6.0 - Convergence

6.1 - Convergence Criteria

A CFX run involves solving a model through a multitude of iterations. It is important to make sure that for every new iteration, the error residuals decrease until eventually they are acceptable. This means that the model has converged. Alternatively, a CFX run can become unstable and cause the error terms to explode and the models to not converge. In this case, the solution is suspect and cannot be relied upon.

To help monitor the CFX runs, two monitor points were created to enable real time observation of how the model converges. These two points were based on the total pressure ratio and the mass balance from inlet to exit. This means that for every iteration of the solution these two points were calculated. This allowed the user to watch a variable converge towards its final solution as CFX settles on a final solution. These points can be an extra check on the validity of the solution.

The time step was chosen using the convergence control length scale option; a conservative setting was selected. The maximum number of iterations was at least two hundred. The convergence criterion was based on maximum residuals, as opposed to root mean square residuals, and it was set to 0.001.

6.2 - Difficulties Encountered

The models did not always reach the convergence criterion of maximum residuals of 0.001. The residuals on some models would decrease until a certain point and then oscillate around that point indefinitely. This would occur especially often on the higher angle IGVs that were more highly separated. When this occurred, as long as the mass balance was correct and the oscillations were stable, the results were accepted.

6.3 - Verification of Accuracy

This was the first time that a CFD analysis was done on the baseline IGV. However, compressor tests have been performed on three different engines with similar IGVs and overall performance data have been collected.

IGV loss was not directly measured in the engine tests but it was possible to infer approximate IGV loss data from the overall compressor tests. Thus, the loss data are not very accurate but they do show the general values and trends. Unfortunately, no data is available beyond 50 degrees of stagger. Three different loss models had been calculated and all three are graphed along with the CFX results for the baseline in Figure 26. The graph shows that the CFX model produced numbers that are similar to the values derived from the tests. For convenience, the baseline is labeled IGV0 and the new designs are IGV1 to IGV10.

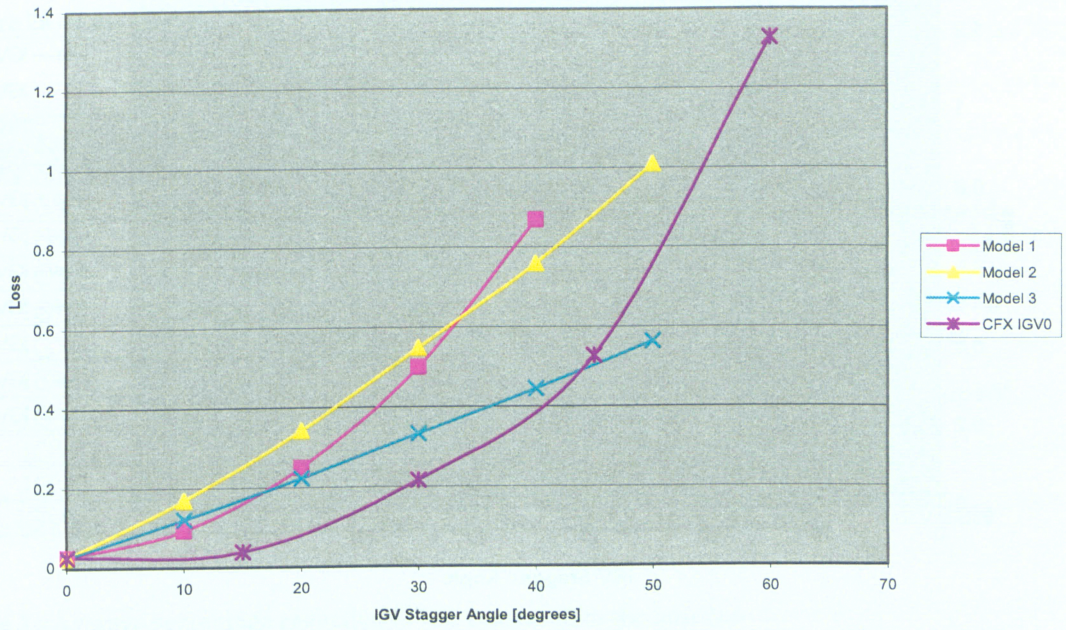

Figure 26 - Loss comparison with test data and existing empirical models

For the new IGVs, there is no way to verify the results apart from checking to make sure the data are sensible. One can partially assume that since the baseline CFX results appear to be reasonably accurate then the other CFX models would be as well.

7.0 – Results & Analysis

7.1 - Loss

The primary variable that was first examined was the total pressure loss coefficient because it is directly linked to changes in efficiency. For each blade, loss was plotted against the IGV stagger angle, seen in Figure 27. Figure 28 shows a close-up of loss against the lower IGV stagger angles for clarity. In general, the new blade shapes increase the loss at the low angles but reduce the loss at the high angles. From Table 3, it can be seen that simply increasing the leading edge radius and the maximum thickness only improved the loss by a small amount. However, the "S" curved IGV significantly lowered the losses at higher stagger angles.

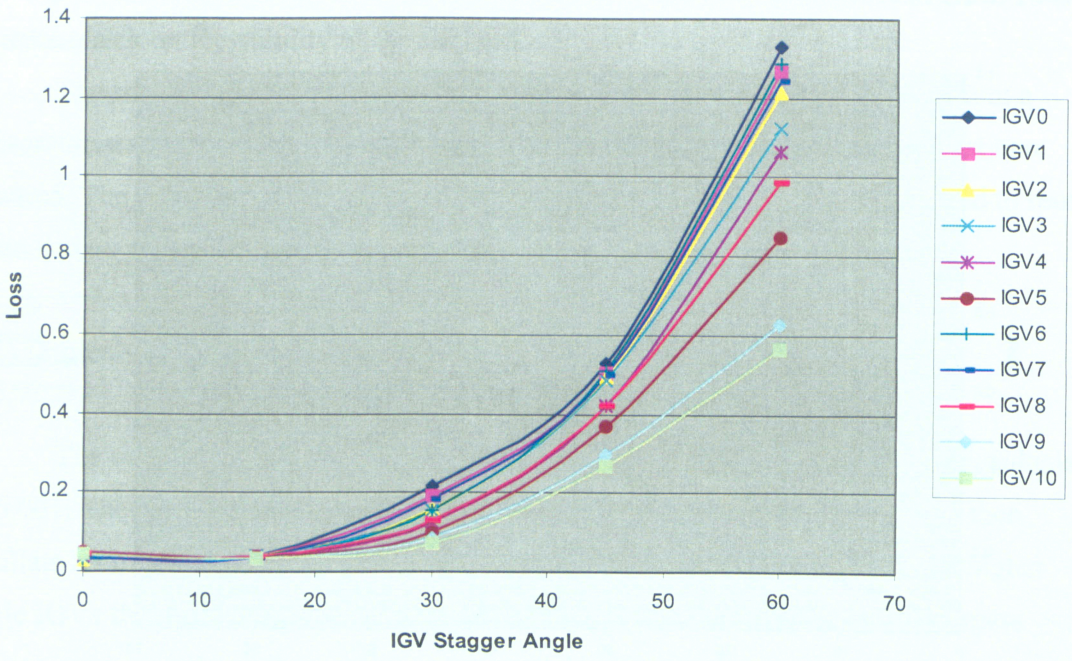

Figure 27 - Loss comparison

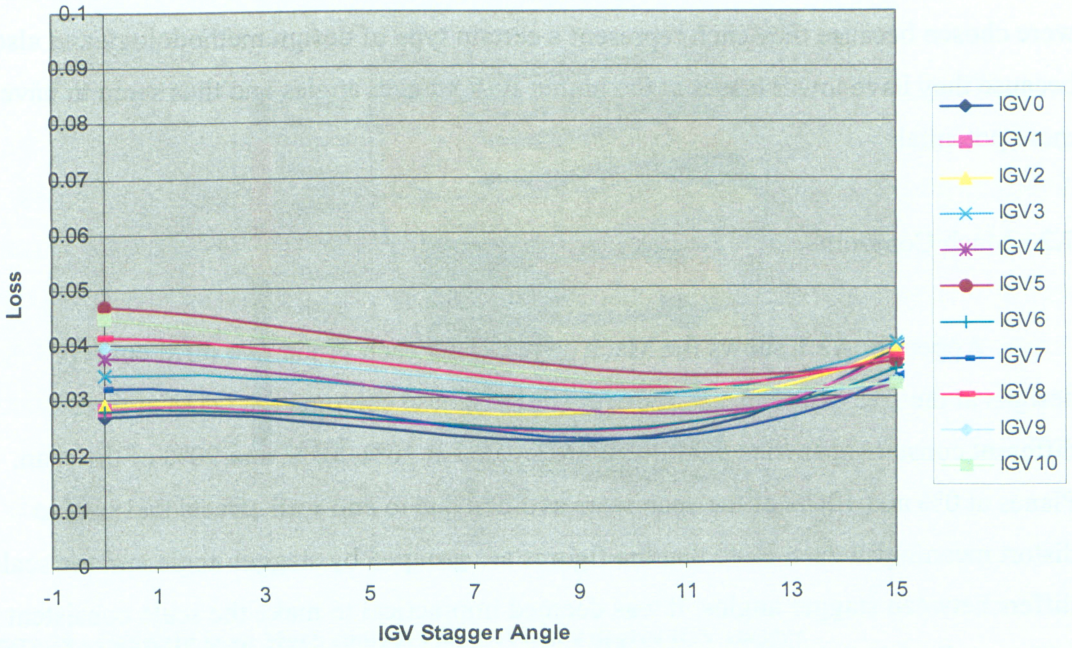

Figure 28 - Loss comparison close-up of low stagger angles

	IGV Stagger Angle					
IGV Version	0	15	30	45	60	Average
IGV1	-5.69%	3.04%	11.96%	4.50%	4.77%	3.71%
IGV2	-7.58%	0.37%	26.68%	6.15%	8.49%	6.82%
IGV3	-27.97%	-2.56%	28.73%	8.08%	15.37%	4.33%
IGV4	-39.86%	17.30%	43.48%	19.88%	19.67%	12.09%
IGV5	-73.80%	6.69%	52.68%	30.19%	36.05%	10.36%
IGV6	-3.78%	9.51%	29.09%	3.54%	3.04%	8.28%
IGV7	-19.89%	13.46%	16.58%	5.74%	6.39%	4.46%
IGV8	-54.16%	4.01%	39.77%	20.42%	25.49%	7.11%
IGV9	-48.18%	16.49%	59.39%	43.32%	52.63%	24.73%
IGV10	-67.14%	16.93%	65.73%	48.74%	57.53%	24.36%

Increased thickness

Increased camber

"Drooped" nose

"S" curvature

Table 3 - Average percentage reduction in loss compared to the baseline

However, Table 3 is misleading, as the IGV does not spend equal amounts of time at each IGV setting. Later, a closer look will be taken at specific missions that the engine would undergo to determine what the actual impact the new design has on net efficiency and specific fuel consumption.

Further analysis will be done on only IGV versions 0, 3, 5, 8, and 10. These IGVs were chosen because they each represent a certain type of design methodology and also because they have lower losses at the higher IGV stagger angles and thus seem to have more potential.

7.2 - Mach Contours

Appendix A2.1 shows the Mach contours for each of the five different IGV designs at the five different IGV stagger angles. These contours are taken at three different constant spanwise planes that are located at 10%, 50%, and 90% of the span. Planes at 0% and 100% of the span were avoided due to end wall effects that tend to distort meaningful data. Note that the figures are grouped by stagger angle and the scale differs between stagger angles. It was deemed impractical to make the scale consistent between all of the graphs because the range would be too large and details would be lost on many of the figures. There is limited value in directly comparing IGVs of different stagger angles because they would be at different mass flows and thus the Mach numbers would be unrelated.

Mach contours are useful to look at because they can indicate areas where losses occur as well as incidence effects. For example, examine Figure 29 and Figure 30. IGV0 has the lowest loss at 0.027 and IGV5 has the highest at 0.047 so it is sensible to compare these two figures. This large difference in loss can be mostly explained by looking closely at the Mach contours. Comparing the mid span plane of both IGVs, it can be seen that on IGV5 the air achieves a higher Mach number. This is even more pronounced towards the shroud. The increase in Mach number could simply be caused by the thicker blade, which increases the metal blockage. Subsonic air speeds up when its area is reduced. If there are sharp speed gradients and the flow is non-uniform then mixing can occur to render the flow uniform again [1]. This mixing can cause an increase in loss. It is preferable to maintain a constant or gradually changing speed to minimize loss.

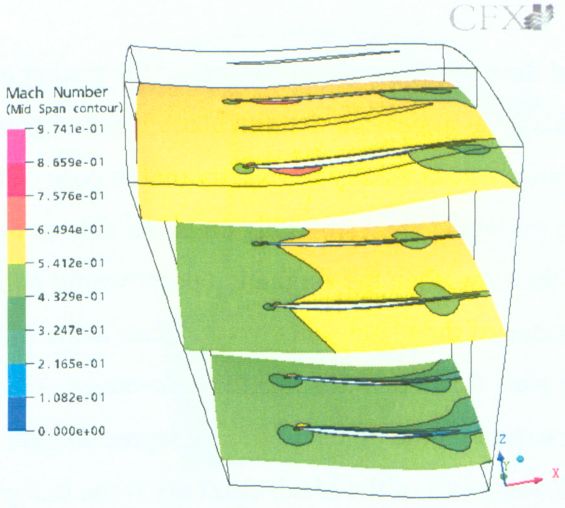

Figure 29 - Constant span Mach contours for IGV0 at 0 degree IGV stagger

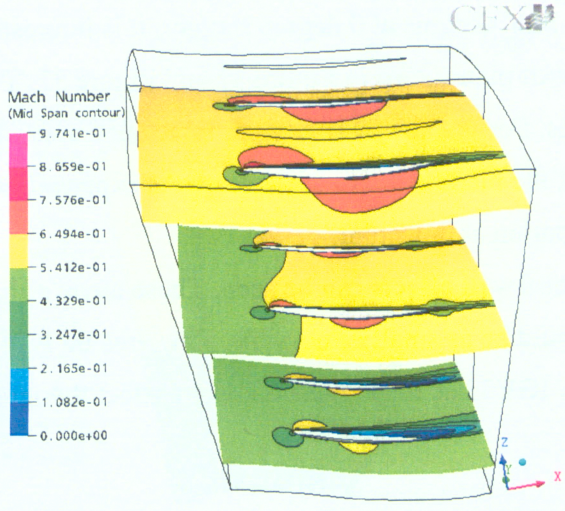

Figure 30 - Constant span Mach contours for IGV5 at 0 degree IGV stagger

Looking at the same figures, it can be seen that there is significant flow separation close to the hub of IGV5. This can be seen by the large area of low velocity flow at the trailing edge of the blade. There is a large pocket of turbulent air that causes the blade shape to effectively be very thick. In general, a thicker blade causes more loss and

decreases the efficiency. Comparatively, IGV0 has a very small amount of this flow separation.

Finally, the last item of note on these figures is the pocket of slower air at the blade leading edge. This is an indication that the blade is not aligned correctly with the flow. The stagnation point would ideally be exactly on the nose of the blade's leading edge [1]. That way the air would flow smoothly on either side of the blade. If the blade were misaligned with the flow, then the stagnation point would either be slightly on the pressure or suction surface of the blade. This would cause some of the flow to speed up and part of the flow to slow down due to streamline curvature. All of these characteristics can be seen to a lesser extent on the other IGVs at 0 degree stagger.

Appendix A2.2 shows all of the Mach contours at the exit plane for zero degree stagger. Ideally, the flow would be uniform over the span. If there were large Mach number gradients then energy would be lost in mixing and it would lower the efficiency of the system. Large distortions in velocity are also detrimental to the efficiency and stall margin of the downstream rotor.

For two of the IGV designs at 0 degree stagger, it is interesting to look at the Mach contours at the exit plane, seen in Figure 31 and Figure 32. Two things are of note looking at these figures. For the new IGV design, there is an area of higher Mach number on the pressure side of the blade close to the shroud. As expected, IGV5 seems to have the worst Mach distribution at this point.

Secondly, the end wall effects can be seen. These areas of low speed near the hub and shroud ideally should be as small as possible. This area on IGV0 is much smaller than the other designs. IGV5 has the biggest end wall effect though IGV10 is also quite bad.

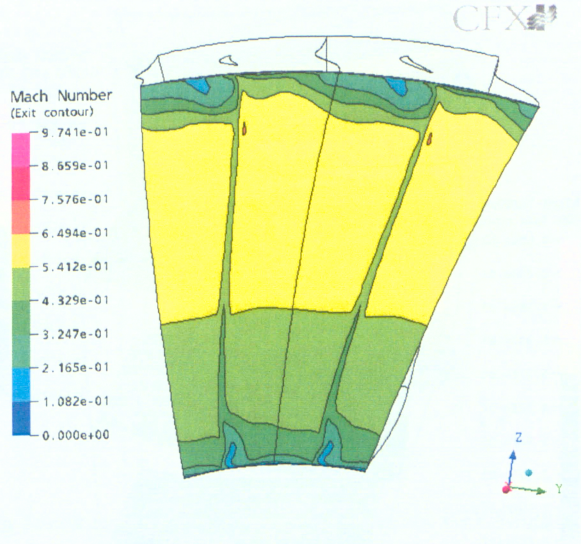

Figure 31 - Mach contour at the exit plane for IGV0 at 0 degree IGV stagger

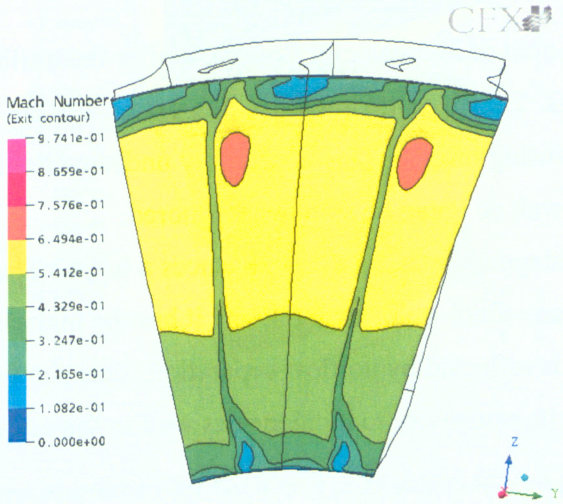

Figure 32 - Mach contour at the exit plane for IGV5 at 0 degree IGV stagger

At a stagger angle of 15 degrees, the losses are quite similar for all of the blades and correspondingly the Mach contours look very similar. There are not major

differences in the Mach contours. IGV0 serves as an example and can be seen in Figure 33.

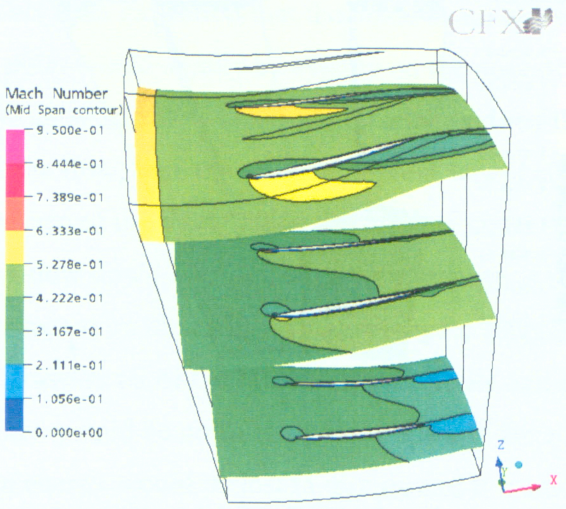

Figure 33 - Constant span Mach contours for IGV0 at 15 degree IGV stagger

Interestingly, an area of low velocity flow right after the trailing edge developed on all of the IGV designs. This may be caused by the suction surface and hub boundary layers interacting and causing mixing. This is certainly undesirable but is apparent in the baseline IGV design as well so it can be somewhat ignored.

For a 30 degree stagger angle, IGV0 experiences a large amount of leading edge separation at the mid span, which helps explain why it has the highest loss. IGV10 has the lowest loss and that is reflected by no flow separation. This shows the effect of leading edge radius and its sensitivity to incidence as well as the advantage of the "S" shape.

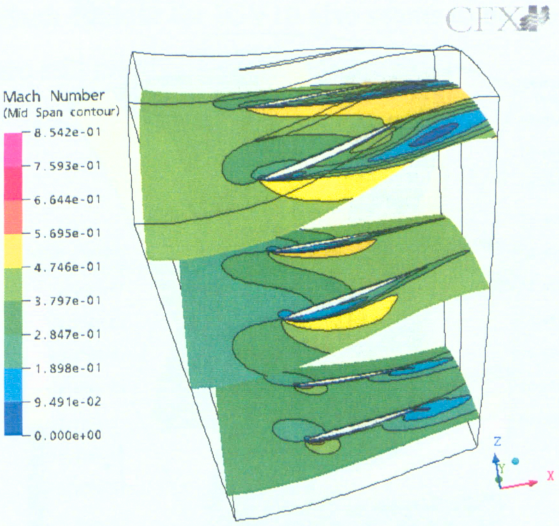

Figure 34 - Constant span Mach contours for IGV0 at 30 degree IGV stagger

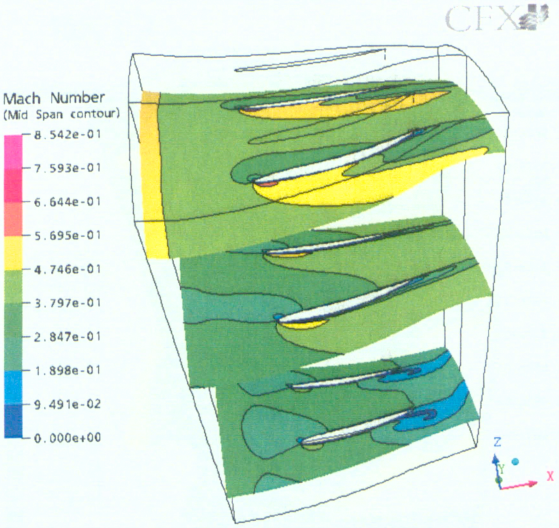

Figure 35 - Constant span Mach contours for IGV10 at 30 degree IGV stagger

The differences in loss are also seen in the exit Mach contours, Figure 36 and Figure 37. IGV0 has a large area of low velocity flow towards the shroud. IGV10 has a much smoother profile. However, it appears that the hub end wall effect of IGV10 is larger than that of IGV0. Presumably, the impact of this larger area of stagnation is of lesser magnitude than the other factors.

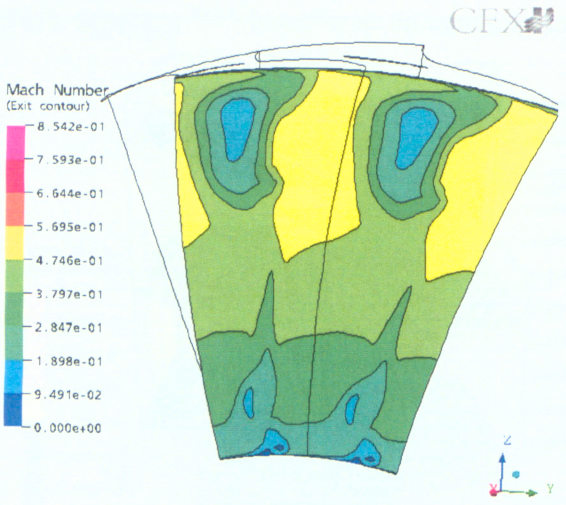

Figure 36 - Mach contour at the exit plane for IGV0 at 30 degree IGV stagger

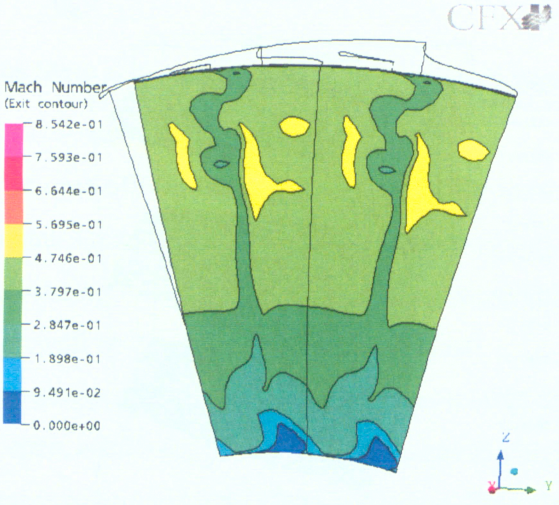

Figure 37 - Mach contour at the exit plane for IGV10 at 30 degree IGV stagger

Stagger angles 45 and 60 are very similar to each other so they will be examined together. The Mach contours are difficult to discern due to high flow distortion, but some trends can be seen. The leading edge separation still appears to be the greatest for IGV0 and the least for IGV10 as seen in Figure 38 and Figure 39. Losses from the leading edge incidence are very difficult to judge in this case as it is very chaotic and so will not be looked at. The exit Mach contours are also informative and they appear in Figure 38 and

Figure 39. The exit Mach contour for IGV10 also seems to be the most uniform though the end wall effects are still relatively large.

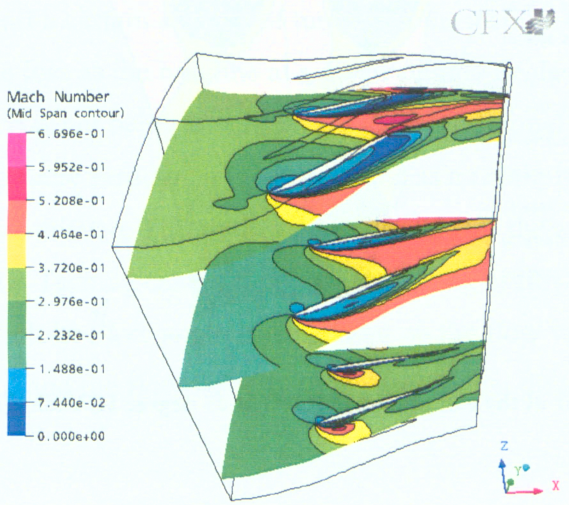

Figure 38 - Constant span Mach contours for IGV0 at 45 degree IGV stagger

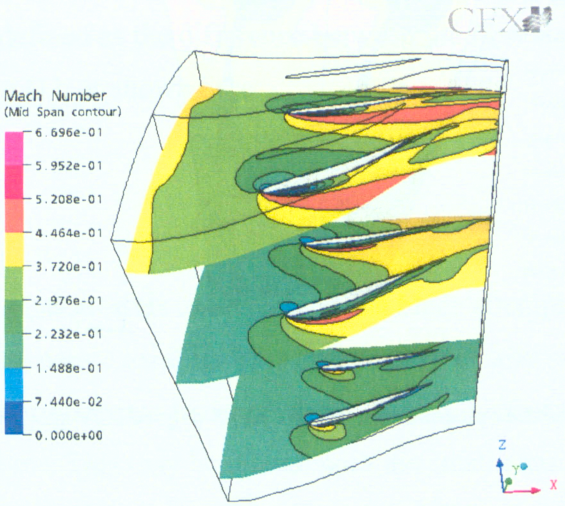

Figure 39 - Constant span Mach contours for IGV10 at 45 degree IGV stagger

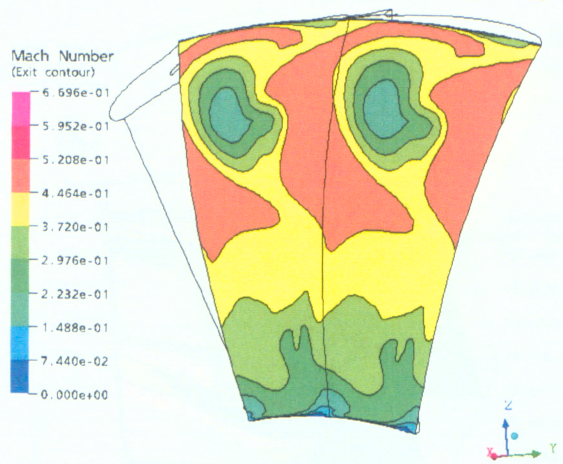

Figure 40 - Mach contour at the exit plane for IGV0 at 45 degree IGV stagger

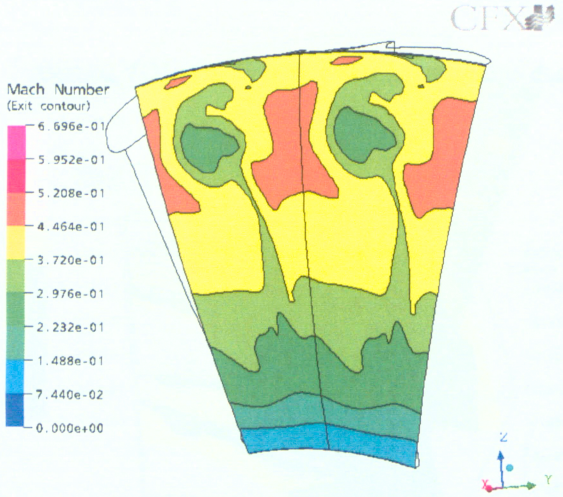

Figure 41 - Mach contour at the exit plane for IGV10 at 45 degree IGV stagger

7.3 – Alpha & Deviation

Loss over the blade is not the only factor in deciding the effectiveness of an IGV. The IGV needs to impart a certain amount of turning in the airflow to be effective. An IGV can have the same loss as the baseline at a given stagger angle but if it is not turning the flow as much then it is not being as effective. In fact, additional stagger may be required to achieve the same aerodynamic turning, and as a result, it is possible that no improvement in loss is achieved. The goal is to try to decrease the amount of loss for the same amount of turning. Turning can be measure by looking at flow angle, α_2, at the trailing edge, defined below. Flow angle is dependent on the flow velocity in the tangential direction, C_u, and the flow velocity in the meridional direction, C_m, both in the stationary frame.

$$\alpha_2 = \tan^{-1}\left(\frac{C_u}{C_m}\right)$$

Deviation is defined as the difference between the flow angle and the blade angle, χ_2, at the trailing edge [1], as shown here:

$$\delta = \alpha_2 - \chi_2$$

In general, deviation tends to increase as the blade attempts to turn the flow more due to increased aerodynamic loading. This trend can be clearly seen in Figure 42. Interestingly, the deviation seems to decrease somewhere between 20 and 40 degrees for most of the IGV designs. This may be related with the small amount of negative incidence that was designed into the original baseline IGV or to perhaps to the onset of separation.

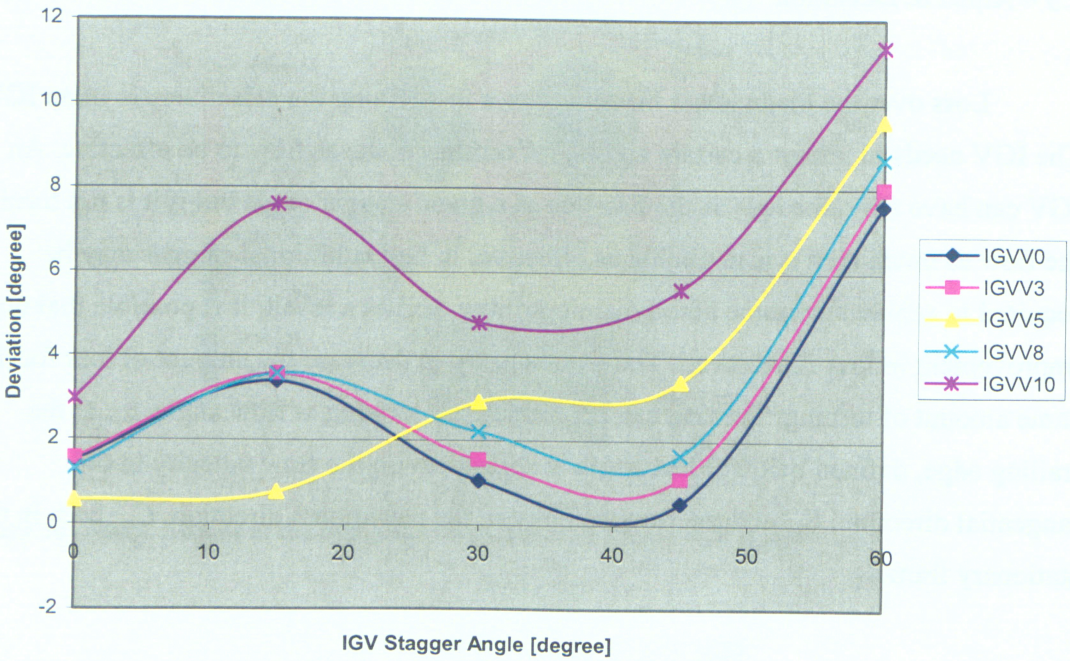

Figure 42 - Deviation

Figure 43 to Figure 47 shows the spanwise profiles of deviation for the different IGV designs at the different stagger angles. In general, deviation increases towards the shroud. This is due to the baseline IGV having more twist towards the shroud compared to the hub and thus all of the IGV designs have this characteristic. The reason for this is that, for the rotors, the blade speed is higher at the shroud due to a larger radius. The IGV imparts a higher swirl at the top in order to reduce the relative Mach number onto the rotor. The end wall effects are very apparent on these figures as well. Boundary layer stagnation normally causes swirl to be poorly defined near end walls so deviations can become very large.

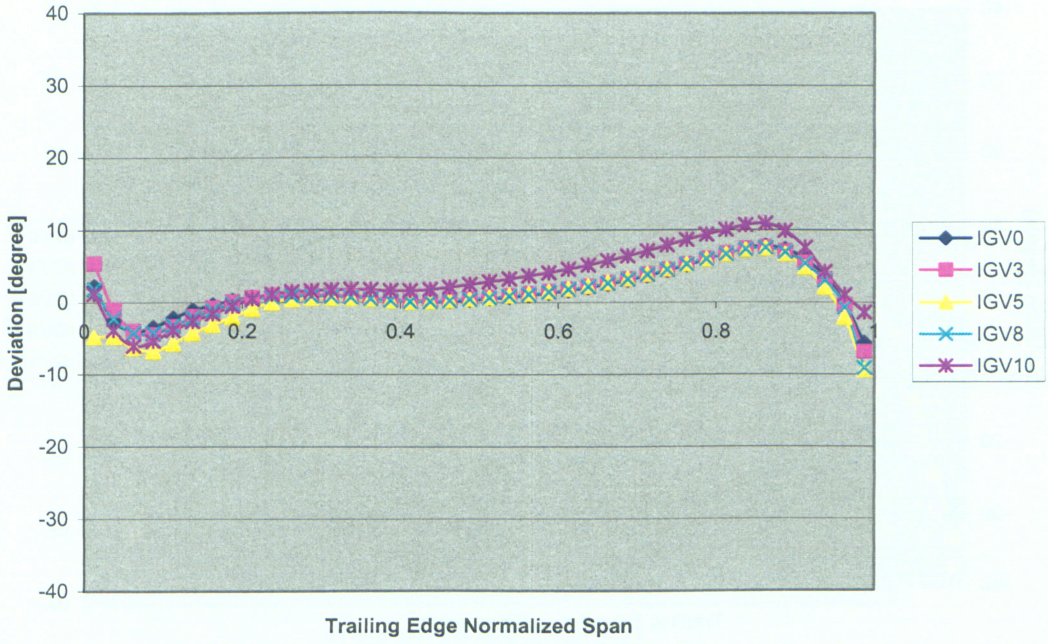

Figure 43 - Spanwise distribution of trailing edge deviation at 0 degree stagger angle

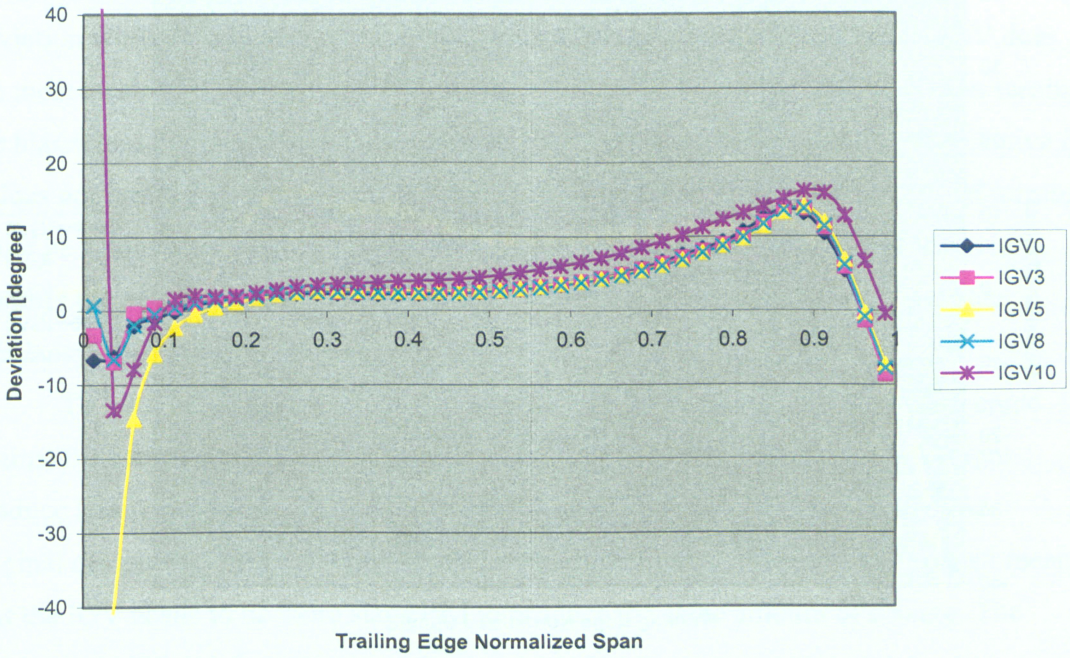

Figure 44 - Spanwise distribution of trailing edge deviation at 15-degree stagger

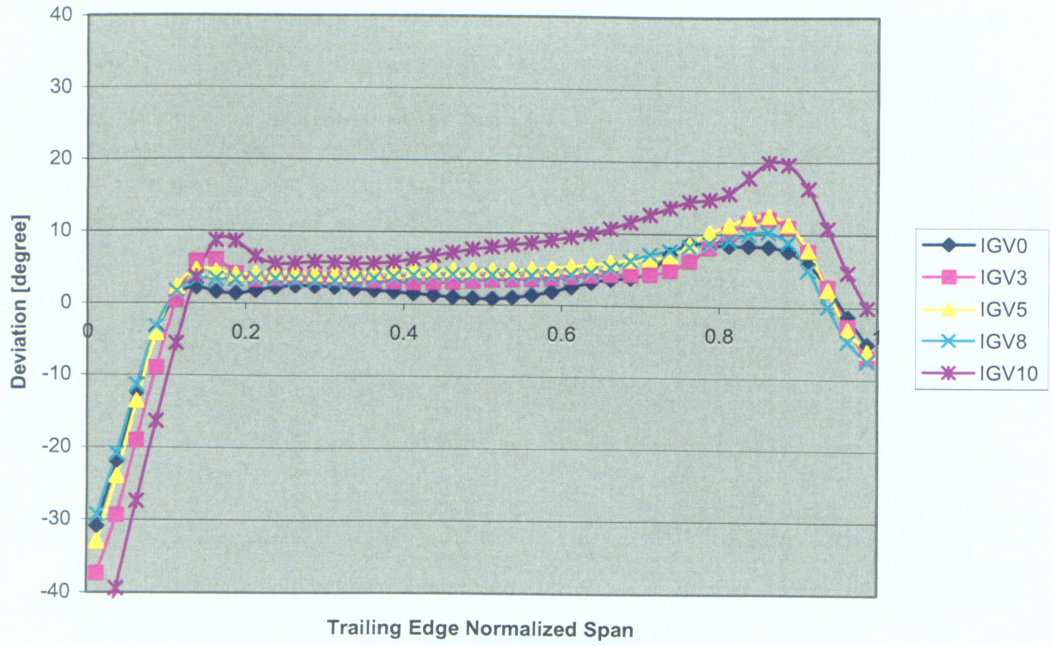

Figure 45 - Spanwise distribution of trailing edge deviation at 30-degree stagger

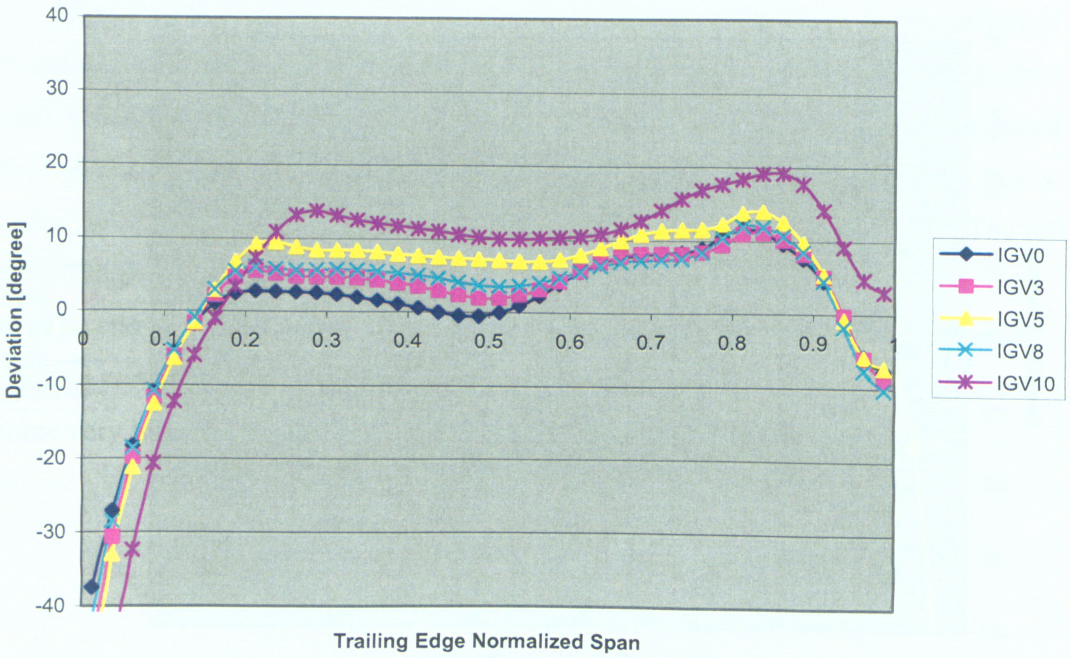

Figure 46 - Spanwise distribution of trailing edge deviation at 45-degree stagger

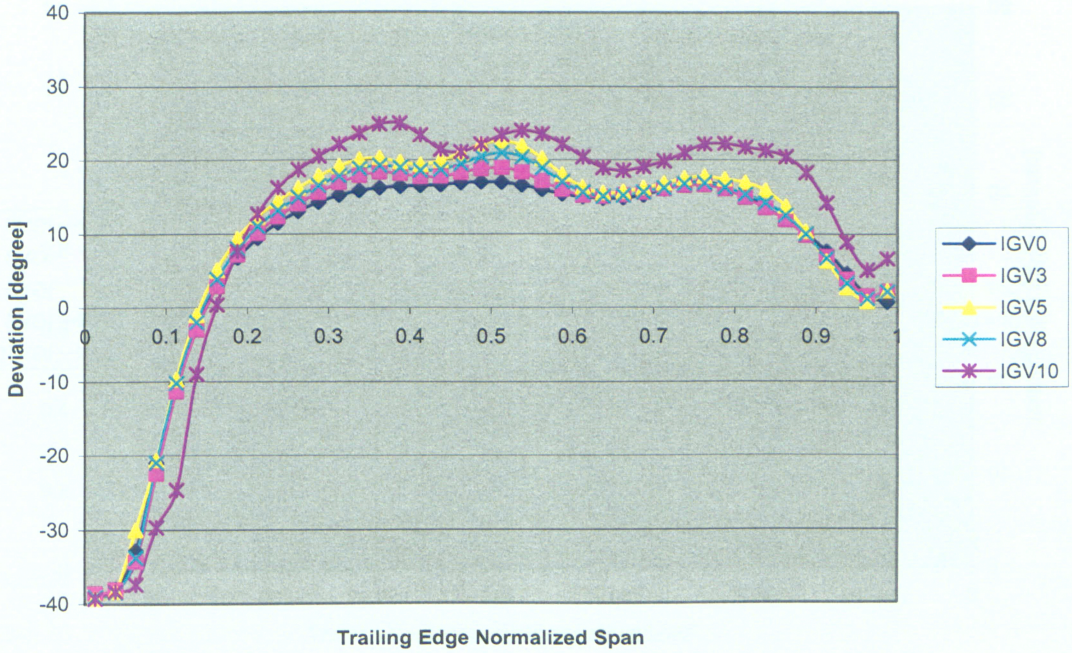

Figure 47 - Spanwise distribution of trailing edge deviation at 60-degree stagger

At all stagger angles, the baseline IGV tends to have the lowest amount of deviation while IGV10 seems to have the most. This implies that the baseline IGV does the most turning at each of these IGV stagger angles. The more deviation, the less turning the blade does. Since turning is the primary purpose of an IGV, a blade is less effective if it does not turn the flow as much. However, it is possible that the same amount of turning could be achieved simply by increasing the stagger angle. The important question is whether the new blade designs can turn the flow the same amount but with a higher efficiency, regardless of the stagger angle.

To get a better understanding of turning, Figure 48 plots the IGV stagger angle against the aerodynamic turning. In general, it can be seen that the new IGV designs produce less turning for a given IGV angle than the baseline. This implies that the original design is superior but that is not necessarily the case. Presumably, this just means that the IGV needs to be more staggered to produce the same amount of turning. The important question is how turning relates to alpha.

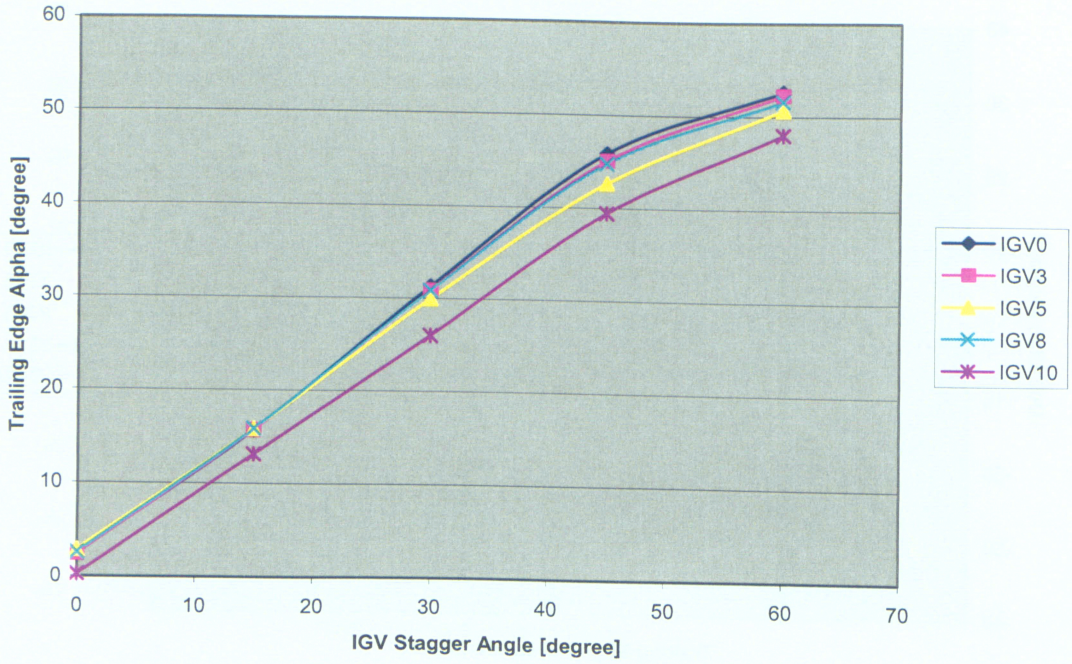

Figure 48 - Average exit alpha

Figure 49 shows the loss plotted against the turning angle for each of the 5 IGV designs. It is apparent that the new IGV designs, especially IGV10, produce less turning for a given IGV stagger angle compared to the baseline. However, it can be seen that the new IGV designs generate lower losses for a given alpha. Unfortunately, the graph is not complete. Since the baseline produces more turning at 60 degree IGV stagger than the newer designs it cannot be proven definitely that the new designs could produce the same amount of turning at a lower loss. That would entail running the IGVs at higher stagger angles, such as 65 or 70 degrees in order to try to achieve the same amount of turning as the baseline at 60 degrees. It is difficult to create these new models though because the mesh is highly skewed at these angles. However, from the shape of the graphs, it appears that the new designs would have a lower loss at that amount of turning though it cannot be said for certain.

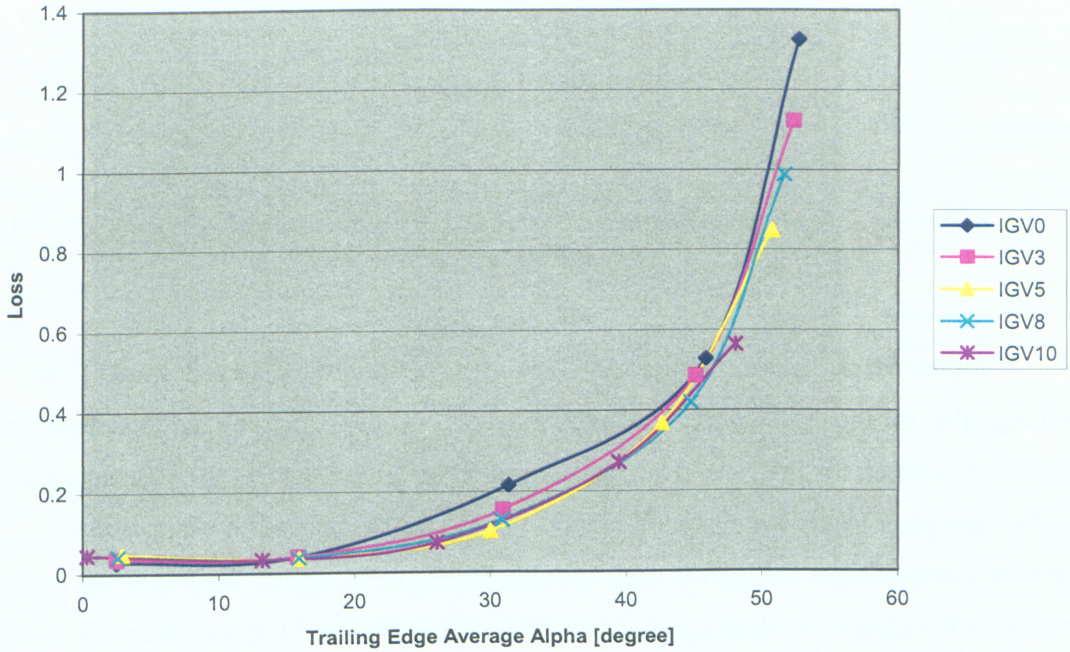

Figure 49 - Turning vs. loss comparison

7.4 – Aerodynamic Blockage Factor

Blockage factor is important because it describes the quality of the flow leaving the control volume. Viscosity causes boundary layers to form along the blade surface and end walls. This causes the effective area to decrease and in turn has a large impact on mass flow. Blockage factor is one way to describe this and the equations used are below [1]. W is the mass flow, T_T is the total temperature, A_{geo} is the geometric area, A_{aero} is the effective aerodynamic area, M_{massAv} is the mass averaged mass flow, γ is the ratio of specific heat capacities, C_D is the discharge coefficient, BF is the blockage factor, and $WTAP$ is the mass flow based on temperature, area, and pressure, either actual or ideal. A sample calculation can be found in Appendix A1.1.

$$WTAPact = \frac{W\sqrt{T_T}}{A_{geo}P_T}$$

$$WTAPideal = WTAPf(M_{massAv}, \gamma)$$

$$C_D = \frac{A_{aero}}{A_{geo}} = \frac{WTAPact}{WTAPideal}$$

$$BF = 1 - C_D$$

Figure 50 compares the blockage factor of a plane immediately following the trailing edge for the different IGV designs. There does not seem to be much difference in blockage between the different designs. However, this graph ignores the blockage factor of the flow prior to the leading edge, which would vary for each case because the boundary condition at the inlet is not explicitly imposed. In reality, the important factor would be the change in blockage factor over the blade. Figure 51 shows the ratio of the trailing edge to leading edge blockage factor versus IGV stagger angle. In this graph, it is quite apparent that the blockage factor for IGV10 is higher than the other IGVs at 0 and 15-degree stagger. At 30 degrees and higher, it actually has the lowest blockage factor and thus provides a less distorted exit flow than all of the other IGVs.

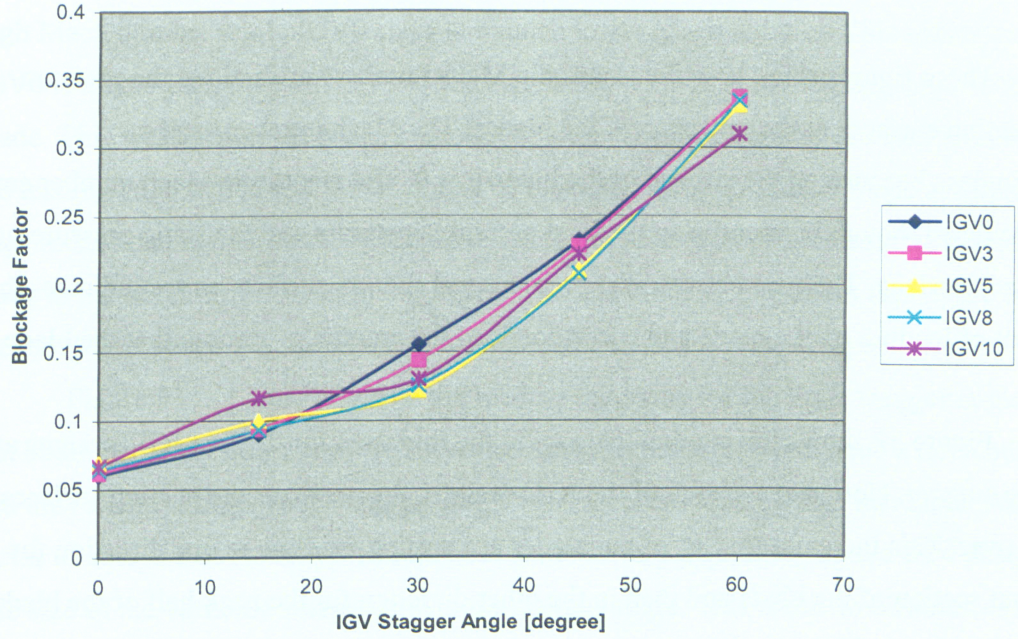

Figure 50 - Blockage factor (calculated just after the blade's trailing edge)

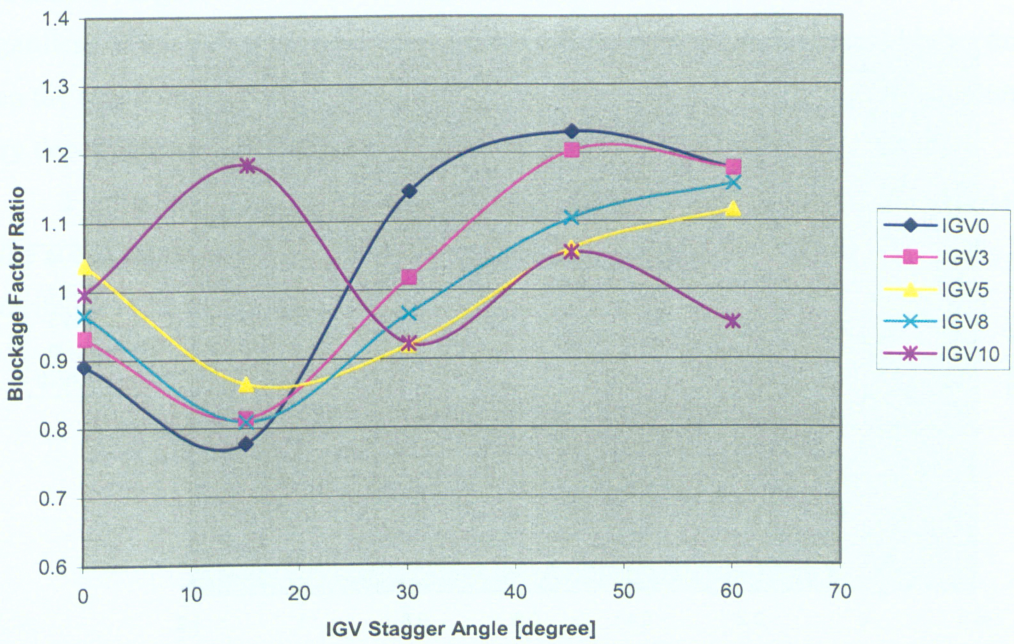

Figure 51 - Blockage factor ratio (calculated just before the leading edge and after the trailing edge)

7.5 – Loading Diagrams

These figures show how the isentropic Mach number varies along the pressure and suction surfaces at the mid span of the blades. The Mach number itself is meaningless because on the surface of the blade it is 0. The isentropic Mach number can be calculated though by measuring the total pressure upstream and the static pressure on the blade surface. The area between the pressure and suction surface curves indicates the amount of loading on the blade and corresponds to the amount of turning that the blade does.

Figure 52 shows the loading diagram at the mid span for the five IGV designs at 0 degree stagger. Note that for each of the IGV designs, the pressure and suction surfaces cross over. This indicates that all of the blades are turning the flow in one direction for the first section of the blade and then in the other direction for the back half of the blade due to incidence. The areas between the curves are approximately the same so they mostly cancel each other out, which indicates no net turning of the air.

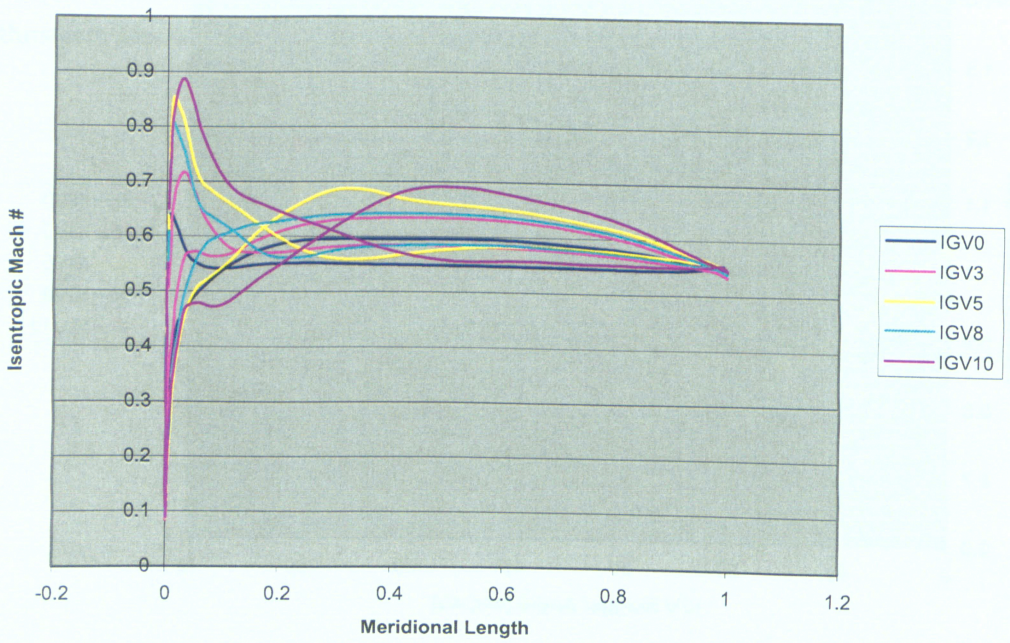

Figure 52 - Isentropic Mach loading diagram at 0 degree stagger and 0.5 span

At the leading edge of the blade, IGV10 and the other new IGVs spike up to a high Mach number while IGV0 stays at a much lower Mach number. This indicates that IGV0 is aligned with the airflow and the stagnation point is at the leading edge of the blade. This was seen in the Mach contours as well. The Mach spikes are also related to the leading edge radius and the thickness of the blade itself. A thicker blade at the leading edge means that the air has to speed up to reach the pressure or suction surfaces and this leads to the Mach spikes seen in the figure. The last thing to note about this figure is that the exit Mach speed is approximately the same for all of the IGV designs.

Figure 53 to Figure 56 show the loading diagrams for the other stagger angles. It can be immediately noted that the curves no longer cross which indicated a net loading and thus a net turning. As the stagger angle increases, the loading also increases. Another factor to note is that the exit Mach number starts to vary depending on the IGV design. The size of the variation increases with the stagger angle. This is due to differences in turning. Since the exit blade angle is the same for all of the blade designs then differences in turning must be due to differences in deviation. IGV0 has the least amount of deviation and thus the highest amount of turning. The axial Mach tends to remain constant regardless of the IGV design because the mass flow is constant. If there is higher turning then the Mach number must be higher as well. This explains why the exit Mach numbers vary depending on IGV design.

Figure 56 shows the loading at 60-degree stagger. It can be seen that the Mach spike at the leading edge for IGV10 is much lower than the other IGVs. This likely contributes to its lower losses.

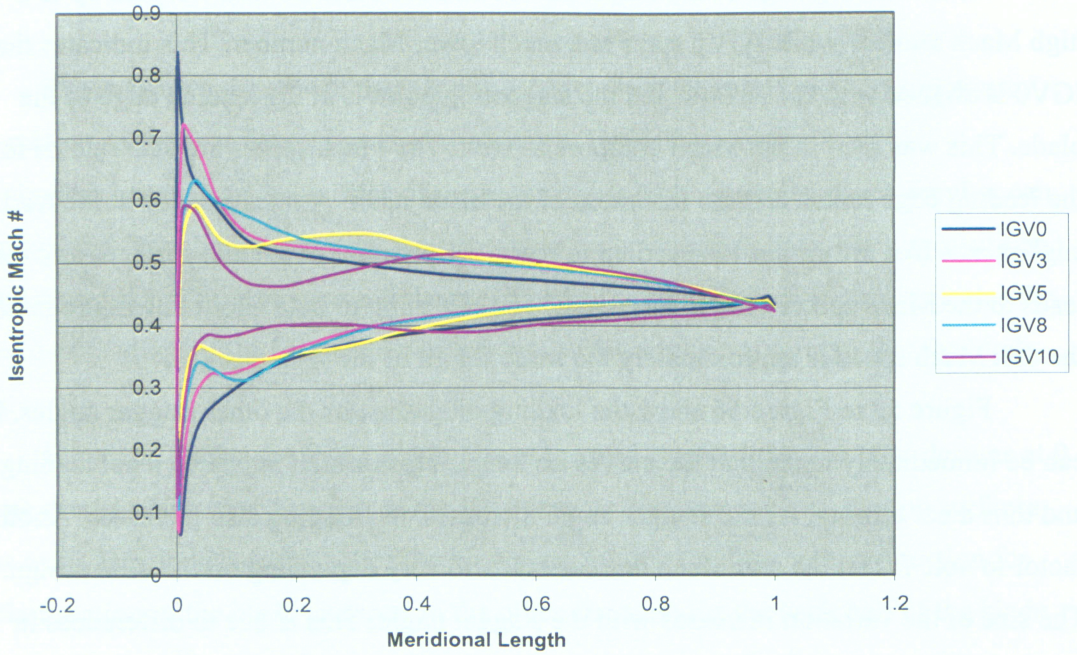

Figure 53 - Isentropic Mach loading diagram at 15-degree stagger and 0.5 span

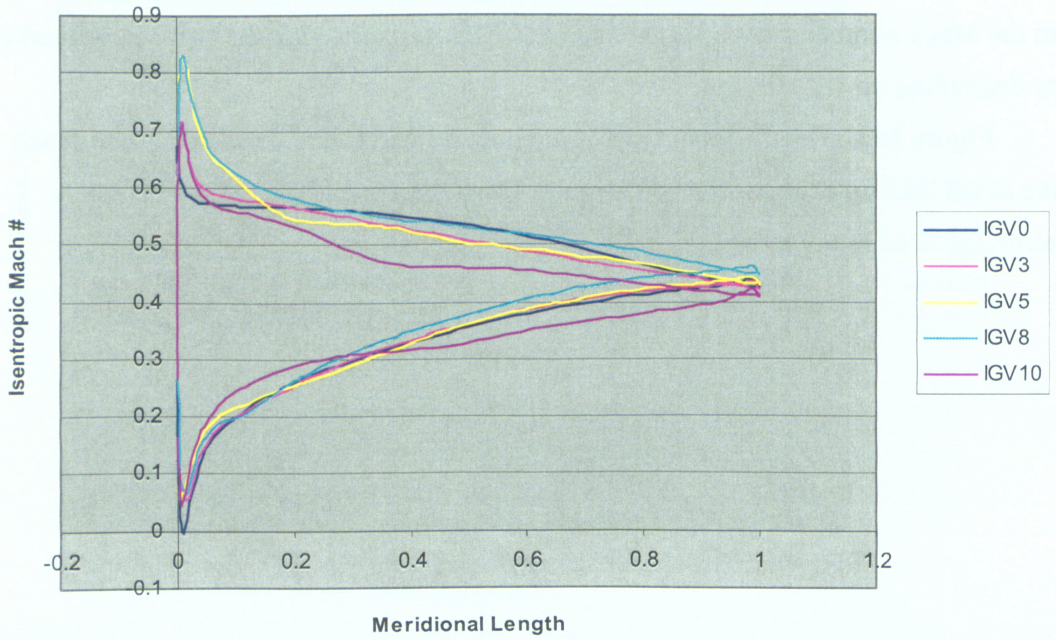

Figure 54 - Isentropic Mach loading diagram at 30-degree stagger and 0.5 span

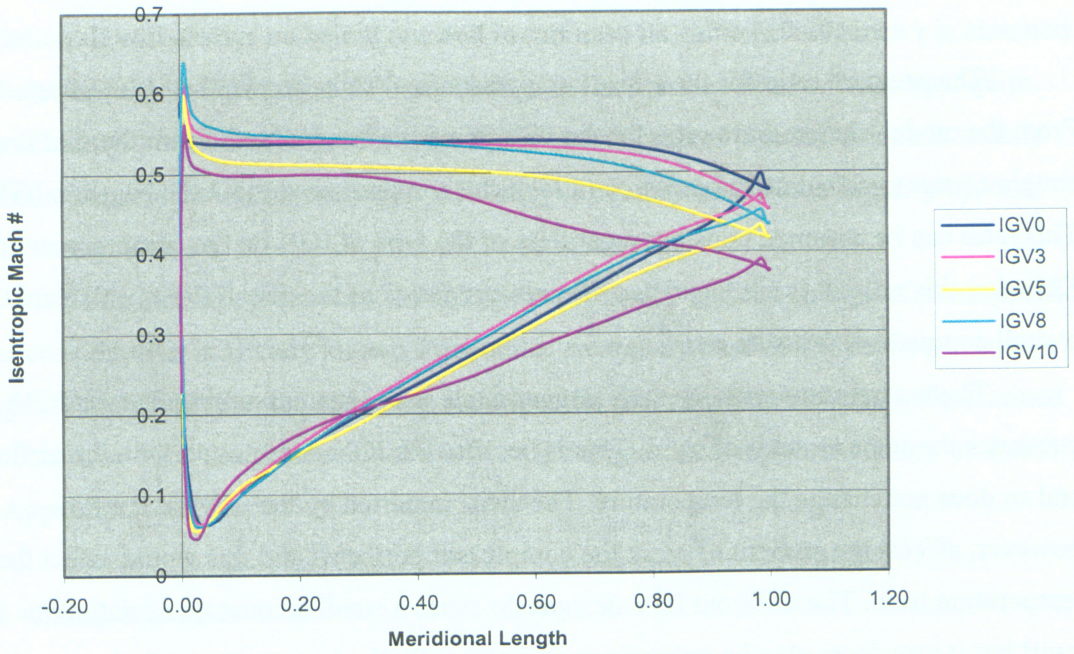

Figure 55 - Isentropic Mach loading diagram at 45-degree stagger and 0.5 span

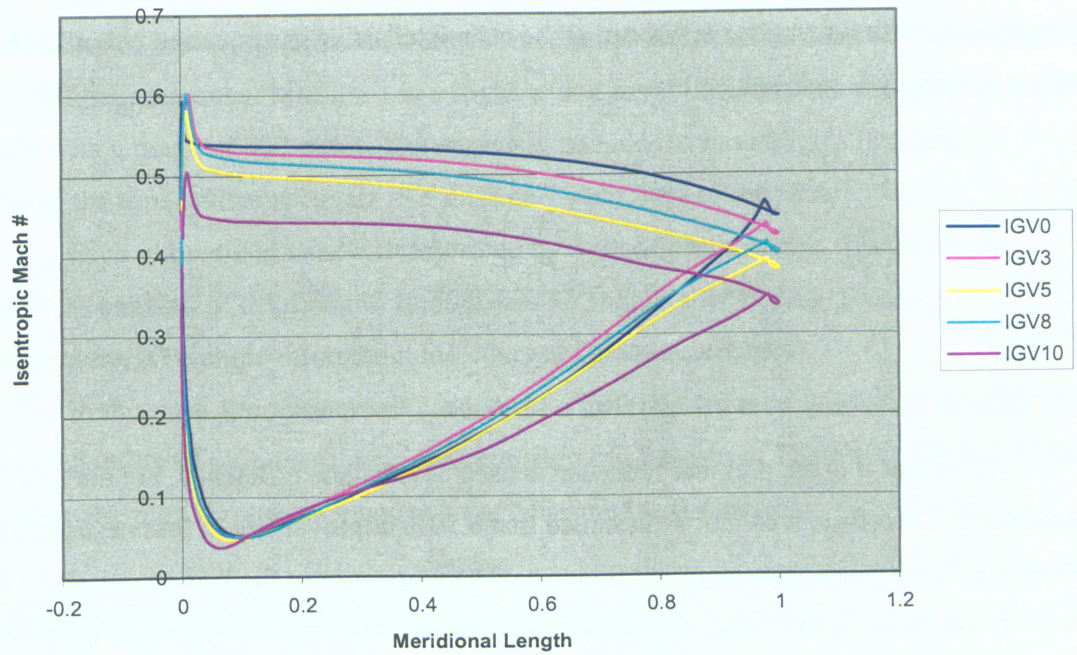

Figure 56 - Isentropic Mach loading diagram at 60-degree stagger and 0.5 span

7.6 – Compressor Efficiency & Fuel Consumption

The pressure ratio for the entire compressor is already known through testing. From the model, the pressure ratio for the IGV itself can be obtained. From there, it is a simple matter to calculate the pressure ratio of the compressor without the baseline IGV. This ratio can be assumed constant regardless of the type of IGV on the compressor. Knowing this ratio, it is simple to use the pressure ratios of the new IGVs to calculate the overall compressor pressure ratio.

The temperature ratio for each stagger angle is constant assuming that the IGV generates the same amount of swirl. This is because the IGV does no work on the airflow and so does not change the temperature. The swirl imparted by the IGV on the flow, however, affects the amount of work the compressor performs and this would affect the temperature ratio. The different IGV designs do cause a small amount of deviation in swirl but it was deemed to be only minor difference. So the temperature ratio is assumed to be constant for each stagger angle and this information is available from P&WC. With all of this information, the efficiency of the baseline compressor and the efficiency of the compressors with the various IGVs can all be calculated using the equation below [15] where efficiency is represented by η.

$$\eta = \frac{\left(\frac{P_{T2}}{P_{T1}}\right)^{\frac{\gamma-1}{\gamma}} - 1}{\left(\frac{T_{T2}}{T_{T1}}\right) - 1}$$

Note that it is the pressure ratio that is used to calculate efficiency, not the loss coefficient. Therefore, it cannot be assumed that a 50% improvement in loss necessarily translates to a 50% improvement in efficiency. The numerator in the loss equation is ΔP_T and it is the driver in this equation because the denominator, dynamic pressure, tends to be fairly constant for the different IGV designs. ΔP_T tends to be quite small compared to the total pressure at any point in the IGV. This means that ΔP_T could be much larger on one IGV compared to another yet the difference in pressure ratio could be very small.

The situation is worsened by the exponent on the pressure ratio in the efficiency equation. It will always be below one and in this case its value is 0.29 since γ is assumed to be equal to 1.4. This means that any change in the pressure ratio is dampened quite significantly. For both of these reasons, significant decreases in loss do not necessarily indicate significant improvements in efficiency. This may be the case in this project as will be seen later on.

The relationship between the change in efficiency and the change of total specific fuel consumption is already known from tables created by the P&WC Performance Department. Therefore, the change in total specific fuel consumption can be determined for each new IGV design at each of the five IGV angles. A sample calculation be found in Appendix A1.2

7.7 - Mission Profiles

P&WC engines are designed for a certain set of missions. A mission set consists of several different individual missions, which do not necessarily have the same probability of occurring. Take for example an engine that has a mission set that consists of 2 different missions. Mission 1 is a flight with a range of 350 miles and mission 2 is a flight with a range of 800 miles. The engine is intended to have flights like mission 1 80% of the time and have flights like mission 2 only 20% of the time.

Each individual mission is described by a set of performance conditions. A condition consists of detailed information on the engine's RPM, inlet pressure and temperature, IGV angle throughout the course of the mission, etc.

In this case, the mission set consists of 4 different types of individual mission. The probability of each these missions occurring can be seen in Table 4. Mission 1 is the shortest and they increase in length so that Mission 4 is the longest.

	Mission 1	Mission 2	Mission 3	Mission 4
Weights	70.00%	15.00%	10.00%	5.00%

Table 4 - Mission breakdown

To simplify the problem, the mission is divided into taxi, take-off, climb, cruise and landing with one running condition representing each stage, as discussed previously. Using interpolation, it is possible to find the change in efficiency due to a new IGV for each of these stages and then a time weighted average of the specific fuel consumption can be calculated. From this information, it is possible to calculate the effect of a different IGV has on the entire mission profile instead of just the IGV at a certain angle. Therefore, it can be seen whether the new IGV has a positive or negative impact on the engine as a whole.

Table 5 summarizes the total fuel consumption change for each IGV design for the different missions. Using the mission weightings, the total change in fuel consumption for the engine is calculated. Surprisingly, all of the new IGV designs have a positive impact on fuel consumption. IGVs 9 and 10 have the best results so it is obvious that the "S" shaped design is the most promising. The drooped nose design generally has the worst results.

	% Reduction in Total Specific Fuel Consumption					
Design	Mission 1	Mission 2	Mission 3	Mission 4	Total	
IGVV1	0.031031	0.008379	-0.002382	-0.00372	0.022554	Increased thickness
IGVV2	0.056049	0.015911	0.015911	0.015911	0.044007	
IGVV3	0.090806	0.010734	-0.022105	-0.026409	0.061643	
IGVV4	0.11368	0.023011	-0.028655	-0.034168	0.078454	Increased camber
IGVV5	0.208159	0.028786	-0.058321	-0.069231	0.140736	
IGVV6	0.020988	0.007459	-0.00073	-0.000967	0.015689	"Drooped" nose
IGVV7	0.033821	0.0027	-0.01673	-0.018234	0.021495	
IGVV8	0.14819	0.017932	-0.043599	-0.051336	0.099496	
IGVV9	0.307873	0.088671	-0.01588	-0.030916	0.225678	"S" curvature
IGVV10	0.334397	0.087338	-0.03382	-0.050605	0.241266	

Table 5 - Percentage reduction in specific fuel consumption

If the results are examined at for each specific mission, then it can be seen that the best results are for the shorter missions. Missions 3 and 4 actually have negative results for some cases.

8.0 - Conclusion

8.1 - Conclusion

The IGV loss can be significantly improved at higher stagger angles, but not without worsening the loss at low stagger angles. With the best IGV design, the engine's overall mission-weighted change in specific fuel consumption improved by 0.24%. This is a small enough change that it is possible that these results are not significant. There is certainly a degree of error in this project due both the assumptions made at the beginning and the difficulty in using CFD to model a turbulent flow.

The four different methodologies used, thicker leading edge, higher camber, drooped nose, and "S" curvature, all lowered the losses at stagger angles higher than 15 degrees compared to the baseline. Below 15 degrees however, they all performed worse than the baseline. Every blade design had a positive impact on the overall engine performance, though in some cases it was a very small improvement.

If the fuel consumption improvements were confirmed to be accurate, it would be worthwhile to investigate the "S" shaped blade further. An improvement of 0.24% may not be very significant but it is likely that with further development this number could be increased.

These results are specific to the given mission profile. If there were an engine that tended to have shorter missions, the new IGV designs would have an even more positive impact on the engine's fuel consumption because of the increased time spent at part power. The opposite is also true in that the new IGVs would perform worse on an engine that operated on longer missions where much of the time was spent near design point.

There are other possible benefits for an IGV that has lower losses at high stagger angles. Some aircraft engines struggle with noise and vibration issues at high IGV stagger angles. One way to possibly reduce this problem is to create a better-behaved flow through the flow path. For IGV10, the airflow at the exit appeared to be more uniform and the blockage factor much lower than that of the baseline. It is possible that one of the new IGV designs could partially or completely alleviate certain noise and vibration problem. Also, lower losses in the IGVs could improve the starting of the engine.

8.2 - Future Work

This paper concentrated on isolating airfoil characteristics that would improve current IGV designs. When possible, no other IGV characteristics were changed when analyzing a new blade design. This is not an optimal way to design an IGV blade. Ideally, the IGV would be completely redesigned with the lessons learned from this project in mind. One would imagine that this methodology would produce a blade that would provide better results.

The "S" shaped airfoil would need further development as well. This project only tested two different curvatures and there is no reason to think that they were necessarily optimal shapes. The idea showed promise though so it would be worthwhile to invest more time in developing that idea further.

Once an IGV was completely redesigned with the concepts learned from this project applied, physical testing would be ideal. CFD is limited in its analysis and so it is always a good idea to confirm the results through experimentation.

9.0 - References

[1] Cumpsty, N A; Compressor Aerodynamics, Longman Scientific & Technical, London, 1989.

[2] Munson, Bruce, Young, Donald & Okiishi, Theodore, "Fundamentals of Fluid Mechanics", Third Edition, John Wiley & Sons, Inc., New York, 1998.

[3] http://www.pwc.ca/en/3_0/3_0_2/3_0_2_3_1.asp

[4] Filippone, A., "Airfoil inverse design and optimization by means of viscous-inviscid techniques", Journal of Wind Engineering and Industrial Aerodynamics, 1995, vol. 56, pg. 123-136.

[5] Sanz, J.M., McFarland, E.R., Sanger, N.L., Gelder, T.F., & Cavicchi, R.H., "Design and Performance of a Fixed, Nonaccelerating Guide Vane Cascade That Operates Over and Inlet Flow Angle Range of 60 Deg", Journal of Engineering for Gas Turbines and Power, April 1985, Vol 107/477.

[6] Tuck, E.O., "A criterion for leading-edge separation", Journal of Fluid Mechanics, 1991, vol. 222, pg. 33-37.

[7] Tuck, E.O. & Dostovalova, A. "Aerofoil nose shapes delaying leading-edge separation", The Aeronautical Journal, September 2000, pg. 433.

[8] Ferguson, T.V. & McGlynn, R.D., "Validation of Turbomachinery Computational Fluid Dynamic Models Using Laser Velocimetry", Journal of IEST, 1999, vol. 42, iss. 6, pg. 19-25.

[9] Denton, J.D. & Dawes, W.N., "Computational fluid dynamics for turbomachinery design", Proceedings of the Institution of Mechanical Engineers, 1999, vol. 213, iss. 2, pg. 107-124.

[10] Barth, T.J. & Jesperson, D.C., "The Design and Application of Upwind Schemes on Unstructured Meshes", AIAA, 1989, Paper 89-0366.

[11] "CFX-5 Manual", Ansys-CFX, 2004.

[12] Roberts, Doug & Steed, Robin, "A Comparison of Steady-State Centrifugal Stage CFD Analysis to Experimental Rig Data", 2004 International ANSYS Conference, 2004.

[13] Sengupta, T.K., De, S., & Gupta, K., "Effect of Free-Stream Turbulence on Flow Over Aerofoil Section at High Incidence", Journal of Fluids and Structures, 2001, vol. 15, pg. 671-690.

[14] Anderson, John D., "Fundamentals of Aerodynamics", Third Edition, McGraw Hill, New York, 2001.

[15] Dixon, S.L., "Fluid Mechanics and Thermodynamics of Turbomachinery", Fourth Edition, Butterworth-Heinemann, Boston, 1998.

A1.0 - Appendix - Sample Calculations

A1.1 - Blockage Factor

In this project, blockage factors were calculated just before and just after the IGV. The following is a hypothetical example calculation.

Given:

$A_{geo} = 4\ in^2$ $\quad T_T = 500\ R$ $\quad M_{massAv} = 0.5$

$W = 0.5\ lb/s^2$ $\quad P_T = 6\ psi$

$$WTAPact = \frac{W\sqrt{T_T}}{A_{geo}P_T} \qquad WTAPact = \frac{0.5\sqrt{500}}{4*6} = 0.4658$$

Gamma is a function of total temperature.

$$\gamma = 1.3835 + 8.8745*10^{-5}T_T - 1.1844*10^{-7}T_T^{\,2} + 1.5469*10^{-11}T_T^{\,3} + 1.5775*10^{-14}T_T^{\,4} - 4.2014*10^{-18}T_T^{\,5}$$

$$\gamma = 1.4011$$

With gamma now know, WTAPideal can be calculated.

$$WTAPideal = WTAPf(M_{massAv}, \gamma) = \frac{M_{massAv}\sqrt{32.17\gamma/53.35}}{\left[\left(1 + \frac{\gamma-1}{2}\right)M_{massAv}^{\,2}\right]^{\frac{\gamma+1}{2(\gamma-1)}}}$$

$$WTAPideal = \frac{0.5\sqrt{32.17*1.4011/53.35}}{\left[\left(1 + \frac{1.4011-1}{2}\right)*0.5^2\right]^{\frac{1.4011+1}{2(1.4011-1)}}} = 16.8585$$

Finally, C_D is a ratio of the two WTAPs.

$$C_D = \frac{A_{aero}}{A_{geo}} = \frac{WTAPact}{WTAPideal} = \frac{0.4658}{16.8585} = 0.02763$$

$$BF = 1 - C_D = 1 - 0.02763 = 0.9724$$

A1.2 - Mission Profiles

Available information at a certain mission condition, for example, at take-off:

RPM = 26000

$\xi = 5°$

$P_{T1} = 20$ psi

$P_{T3} = 300$ psi

$T_{T1} = 600$ R

$T_{T3} = 1500$ R

From this, the pressure and temperature ratios as well as the efficiency over the compressor can be calculated. The compressor includes the IGV as well.

$$\left(P_{T3}/P_{T1}\right)_5 = 15 \qquad \left(T_{T3}/T_{T1}\right)_5 = 2.5$$

$$\eta_5 = \frac{\left(\frac{P_{T3}}{P_{T1}}\right)_5^{\frac{\gamma-1}{\gamma}} - 1}{\left(\frac{T_{T3}}{T_{T1}}\right)_5 - 1} = \frac{15^{(1.4-1/1)} - 1}{2.5 - 1} = 0.7786$$

This is the efficiency of the baseline at an IGV stagger angle of 5 degrees. Future IGV designs at the same conditions will be compared to this value.

The following information is available from the CFX baseline cases that were examined at the different stagger angles. Recall that the pressure ratio is over the IGV only.

IGV Angle	P_{T2}/P_{T1}
0	0.995844
15	0.995866
30	0.985442
45	0.977708
60	0.968607

The mission condition that is being examined was at take-off where the IGV is at 5 degrees. Linear interpolation is used to calculate the pressure ratio that corresponds to that IGV setting.

$$\frac{\xi_{15}-\xi_0}{\left(P_{T2}/P_{T1}\right)_{15}-\left(P_{T2}/P_{T1}\right)_0}=\frac{\xi_{15}-\xi_5}{\left(P_{T2}/P_{T1}\right)_{15}-\left(P_{T2}/P_{T1}\right)_5}$$

$$\frac{15-0}{0.995866-0.995844}=\frac{15-5}{0.995866-\left(P_{T2}/P_{T1}\right)_5}$$

$$\left(P_{T2}/P_{T1}\right)_5=0.995851$$

Efficiency cannot be calculated over an IGV, it must be calculated over the compressor, which includes the IGV. The pressure ratio over the compressor without the IGV remains constant and it can be easily obtained.

$$\frac{P_{T3}}{P_{T2}}=\frac{P_{T3}}{P_{T1}}*\frac{P_{T1}}{P_{T2}}=15*\frac{1}{0.995851} \qquad \frac{P_{T3}}{P_{T2}}=15.0625$$

This pressure constant is true regardless of the IGV design. It is now possible to take the pressure ratio over a new IGV design and calculate the pressure ratio over the

compressor as a whole. This way it will be possible to compare the efficiencies of compressors that have different IGV designs. The following is an example of this.

The information below is from CFX and it is for IGV10.

IGV Angle	P_{T2}/P_{T1}
0	0.993056
15	0.996554
30	0.994168
45	0.987384
60	0.983788

As before, the compressor is being examined at take-off where the IGV stagger angle is 5 degrees. Once again, linear interpolation is needed.

$$\frac{15-0}{0.993056-0.996554}=\frac{15-5}{0.993056-\left(P_{T2}/P_{T1}\right)_5}$$

$$\left(P_{T2}/P_{T1}\right)_5 = 0.995388$$

As before, the pressure ratio over the entire compressor with IGV can now be calculated.

$$\frac{P_{T3}}{P_{T1}}=\frac{P_{T3}}{P_{T2}}*\frac{P_{T2}}{P_{T1}}=15.0625*0.995388$$

$$\frac{P_{T3}}{P_{T1}}=14.9930$$

The temperature ratio over the compressor is independent of the IGV so it is the same value as before. With all of this information, the efficiency can now be calculated.

$$\eta_5 = \frac{\left(\frac{P_{T3}}{P_{T1}}\right)_5^{\frac{\gamma-1}{\gamma}} - 1}{\left(\frac{T_{T3}}{T_{T1}}\right)_5 - 1} = \frac{14.9930^{(1.4-1/1.4)} - 1}{2.5 - 1} = 0.7784$$

The change in efficiency is then calculated to be:

$$\Delta\eta = 0.7786 - 0.7784 = 0.0004$$

The relationship between the change in efficiency and the change in fuel consumption of the engine was available. For example, it could be that for every 0.01 change in efficiency, the total fuel consumption would change by 0.5%. Knowing this, it is a simple matter to calculate the change in fuel consumption comparing a new IGV design to the baseline.

$$\Delta FC = 0.0004 * 0.5\% = 0.0002\%$$

These calculations would be performed on all of the different conditions that would constitute a mission, such as taxiing, takeoff, climb and cruise. A time-weighted average of the change in fuel consumption would then be calculated. This would be very simple, as the time spent at each of these conditions would be known. Afterwards, the different types missions that an engine would fly would also have to be looked at. Finally, a time-weighted average of the fuel consumption for all of the missions would be calculated. This means that there would be one number that represents the overall change in fuel consumption for the engine with a new IGV.

A2.0 - Appendix - Mach Contours

A2.1 - Spanwise View

At 0 degree stagger:

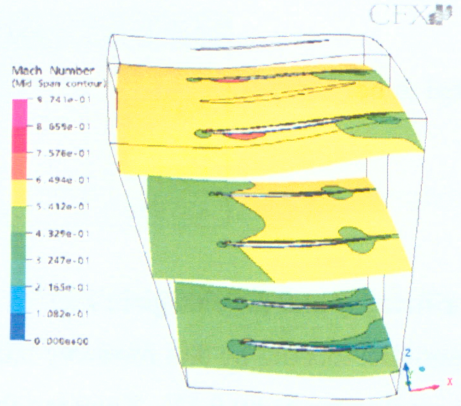

IGVV0

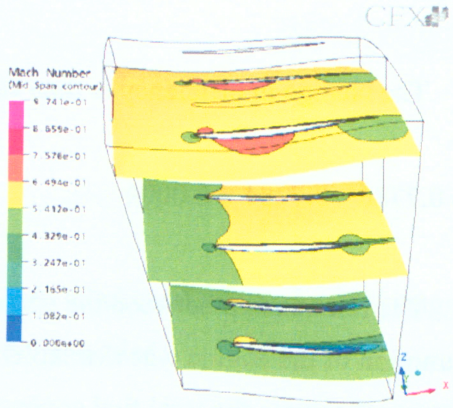

IGVV3

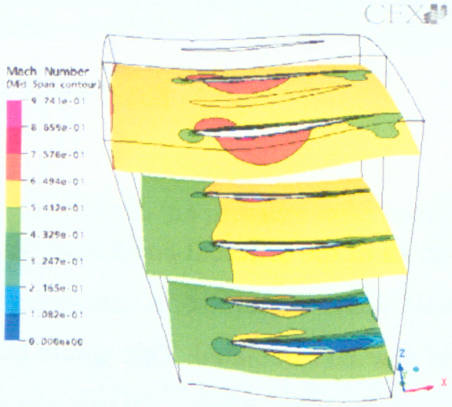

IGVV5

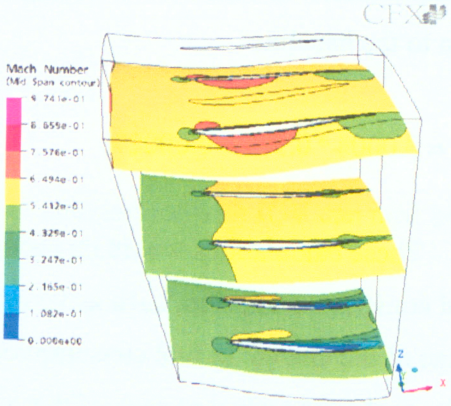

IGVV8

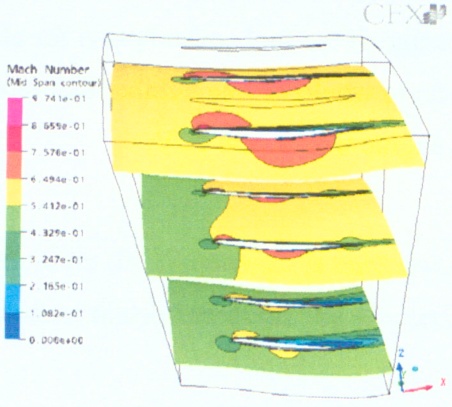

IGVV10

At 15 degree stagger:

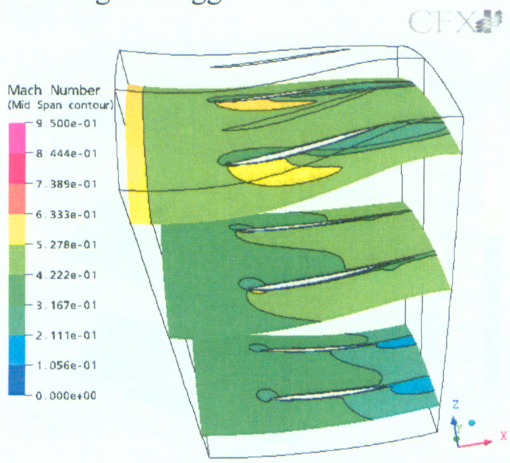

IGVV0

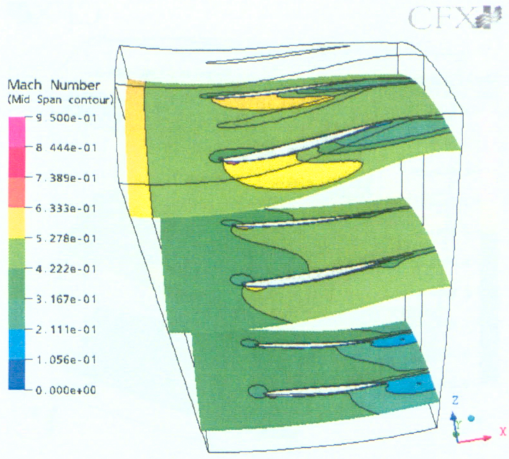

IGVV3

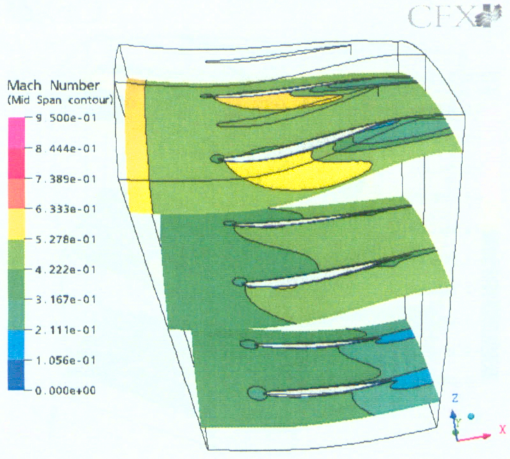

IGVV5

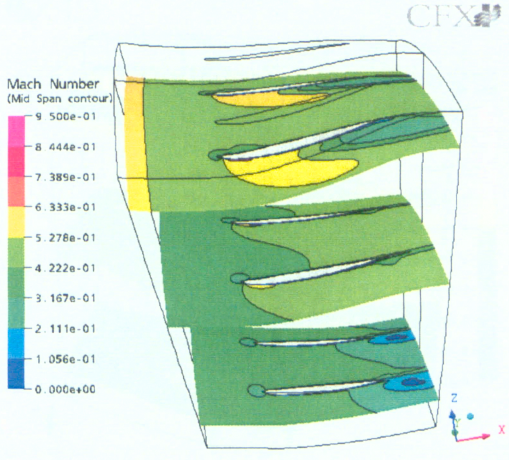

IGVV8

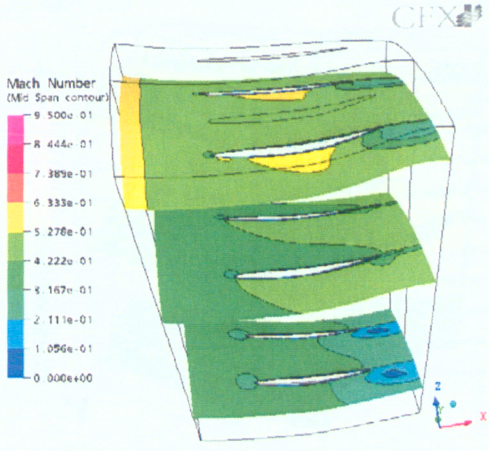

IGVV10

At 30 degree stagger:

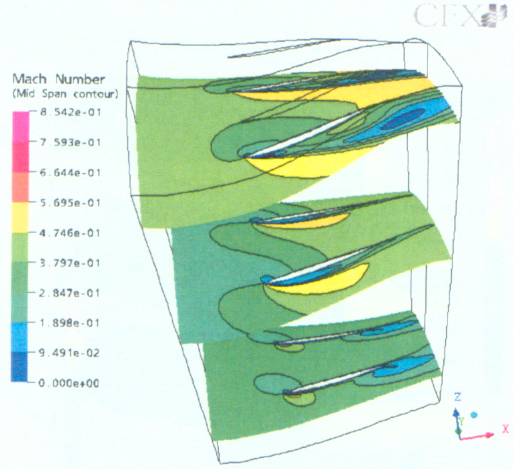

IGVV0

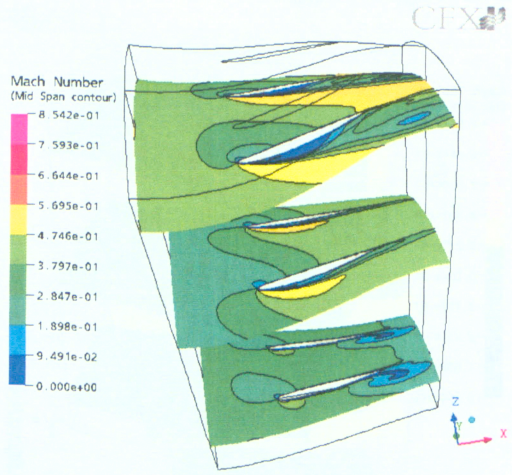

IGVV3

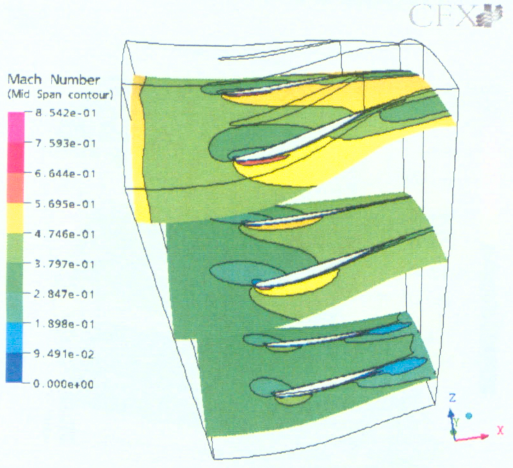

IGVV5

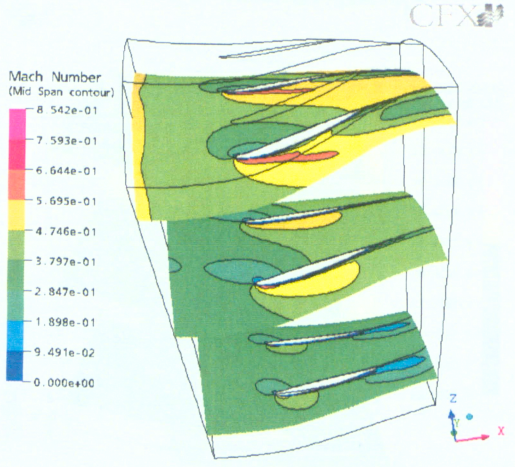

IGVV8

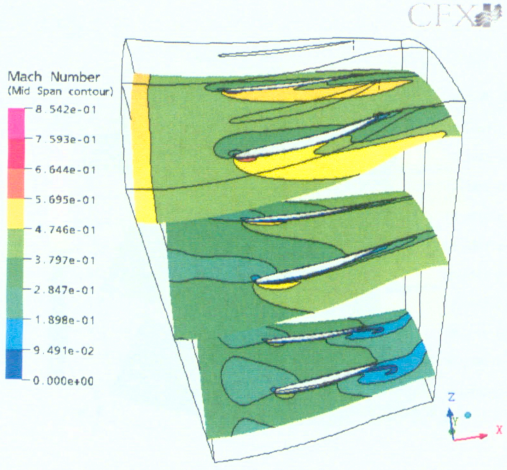

IGVV10

At 45 degree stagger:

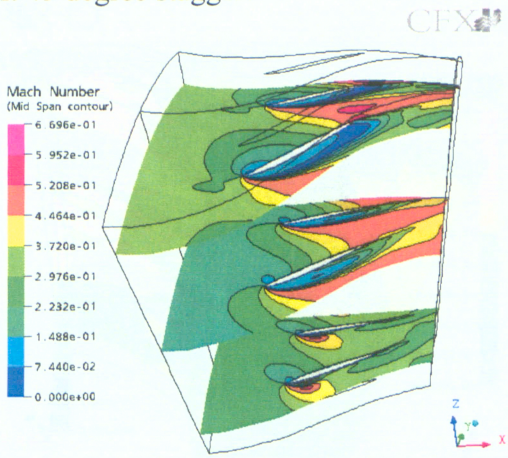

IGVV0

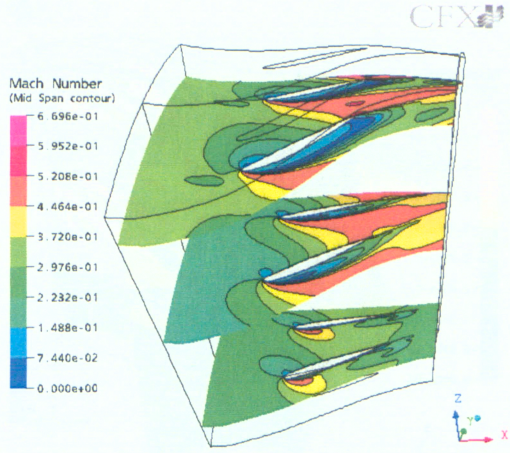

IGVV3

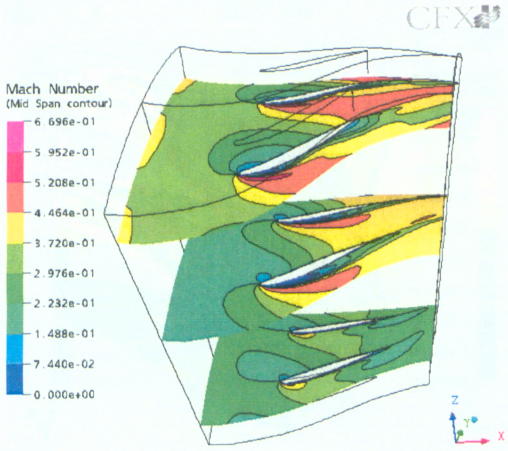

IGVV5

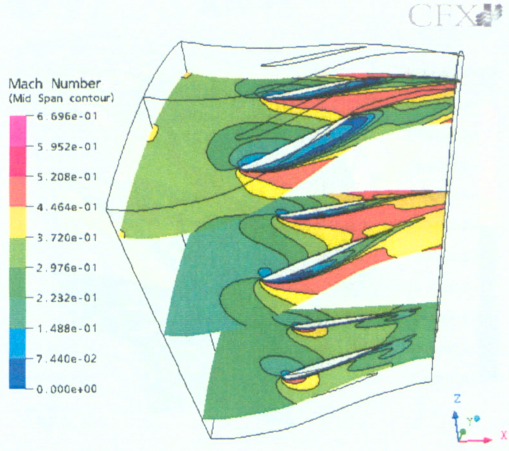

IGVV8

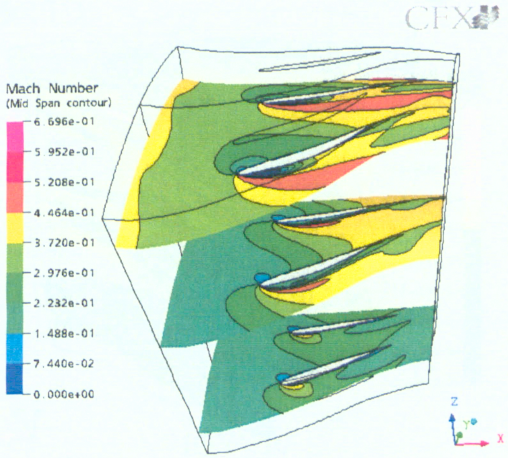

IGVV10

At 60 degree stagger:

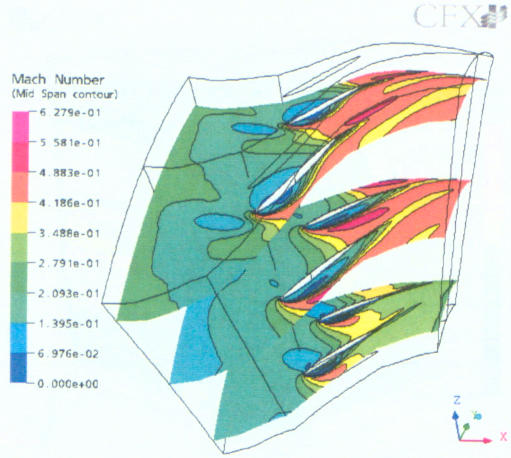

IGVV0

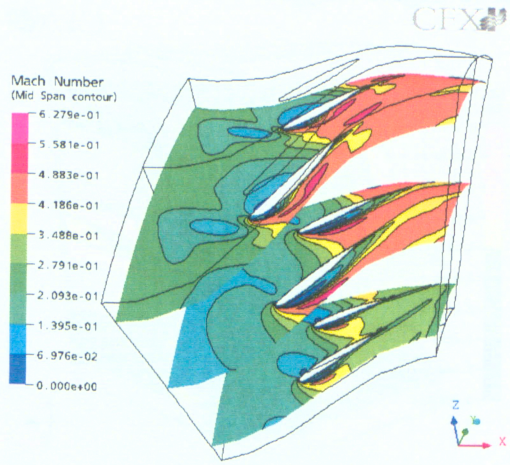

IGVV3

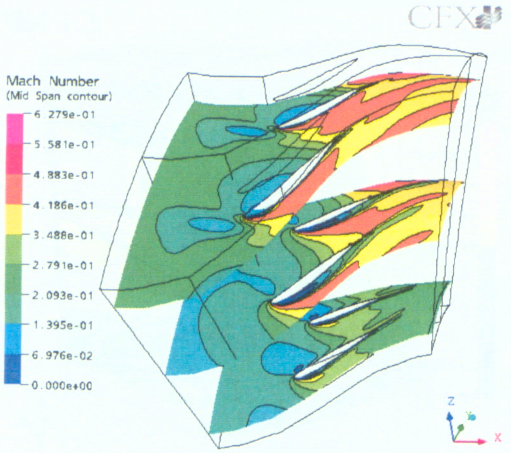

IGVV5

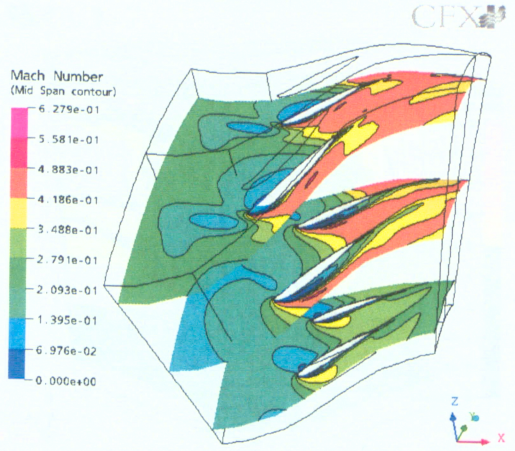

IGVV8

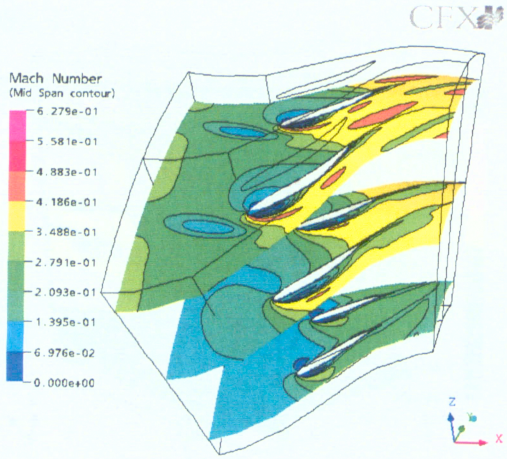

IGVV10

A2.2 - Exit View

At 0 degree stagger:

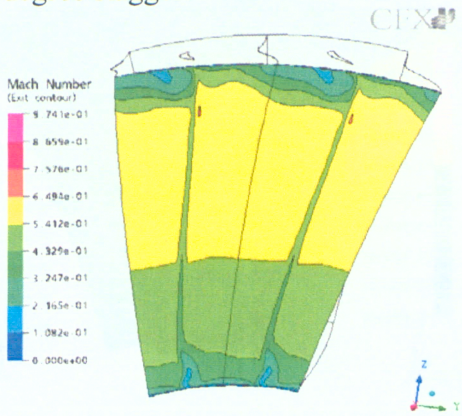

IGVV0

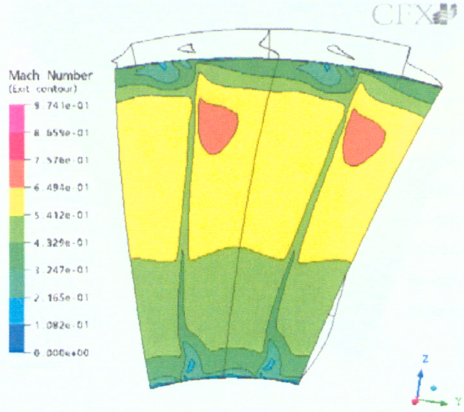

IGVV3

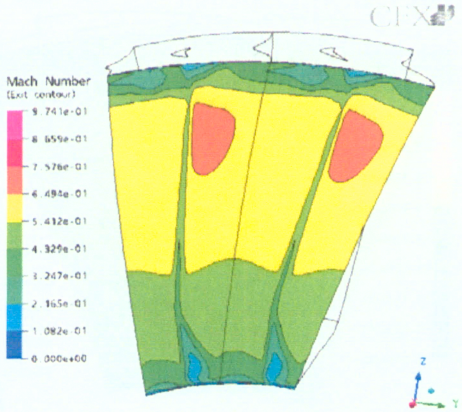

IGVV5

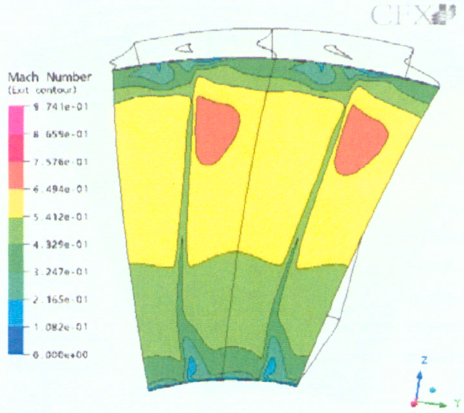

IGVV8

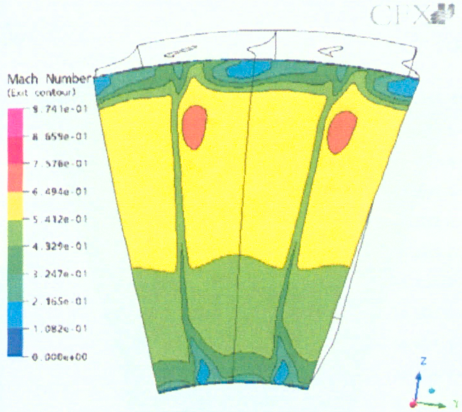

IGVV10

At 15 stagger:

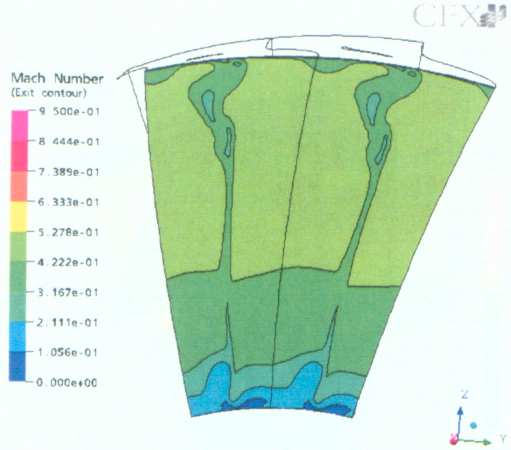

IGVV0

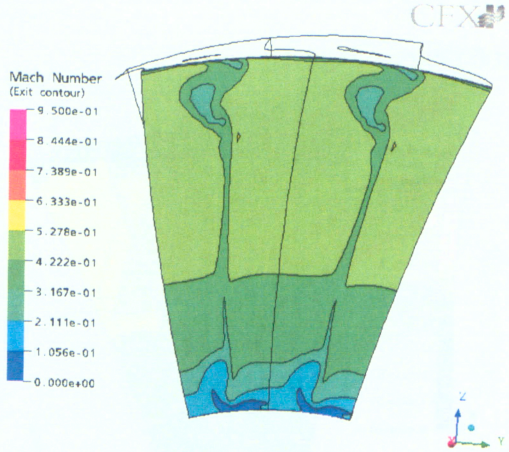

IGVV3

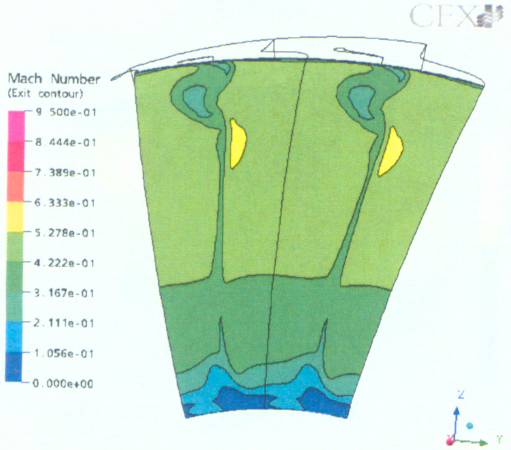

IGVV5

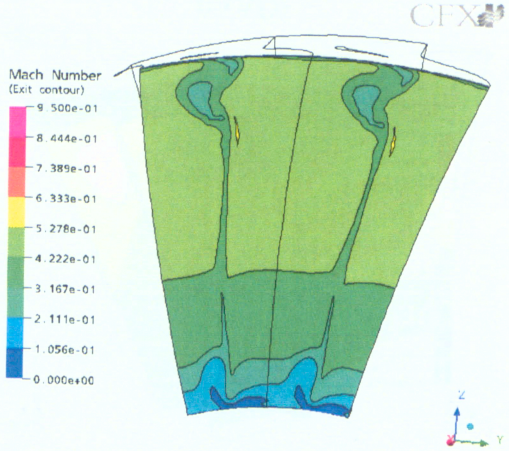

IGVV8

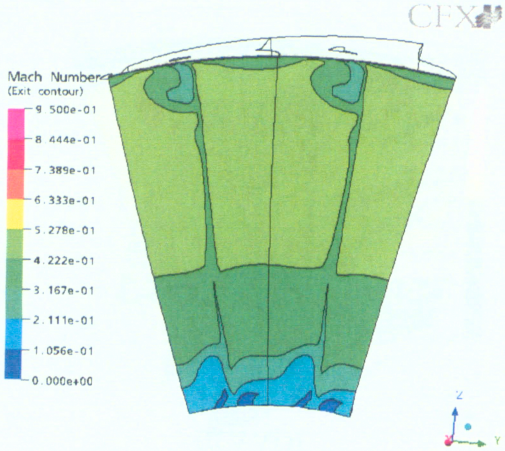

IGVV10

At 30 degree stagger:

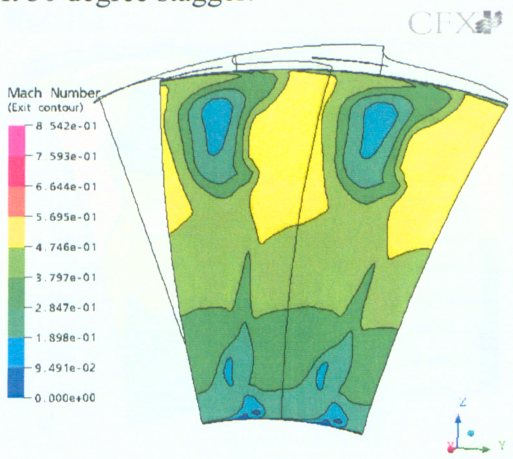

IGVV0

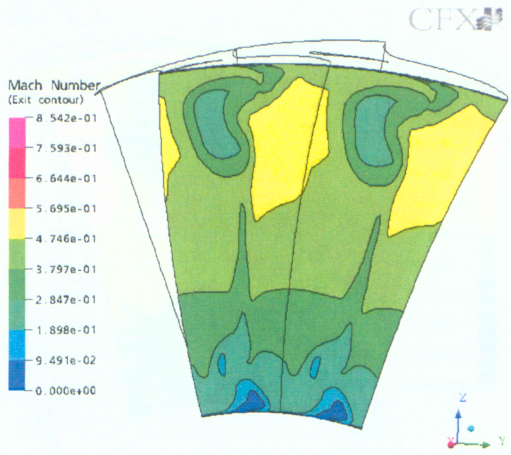

IGVV3

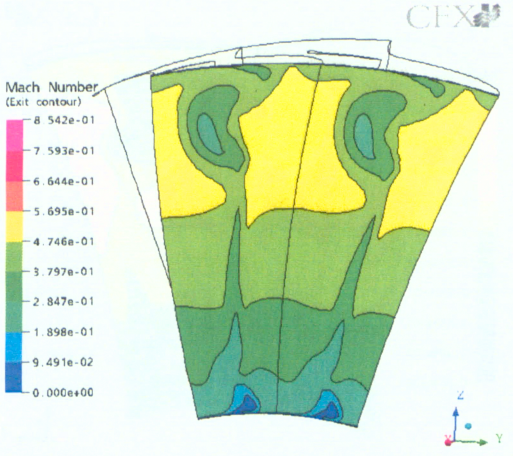

IGVV5

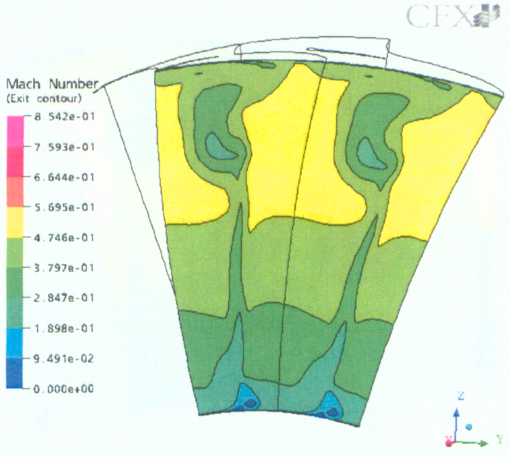

IGVV8

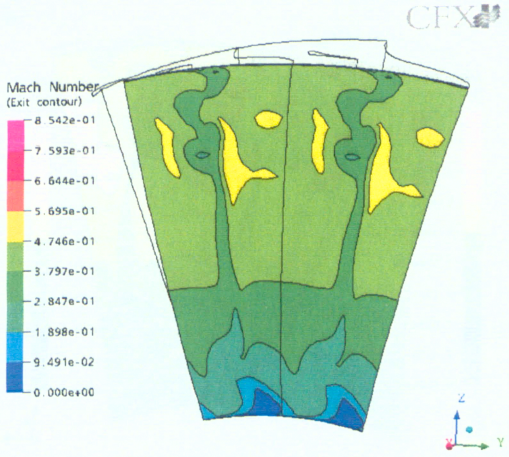

IGVV10

At 45 degree stagger:

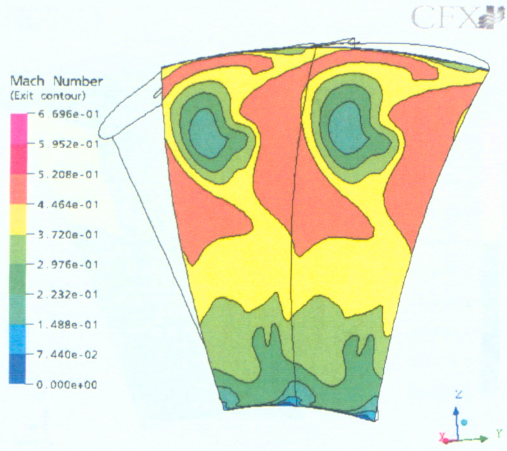

IGVV0

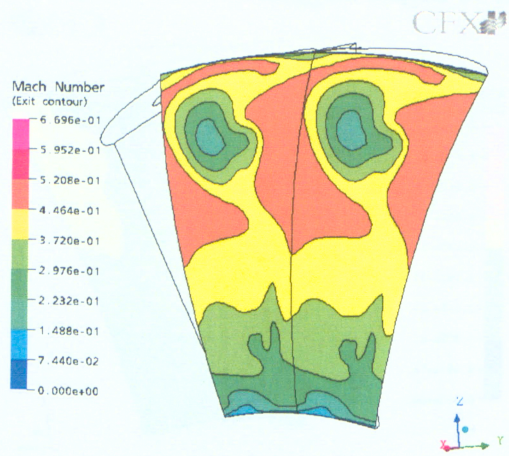

IGVV3

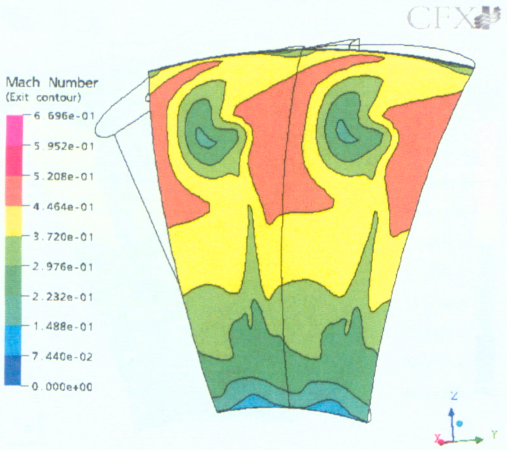

IGVV5

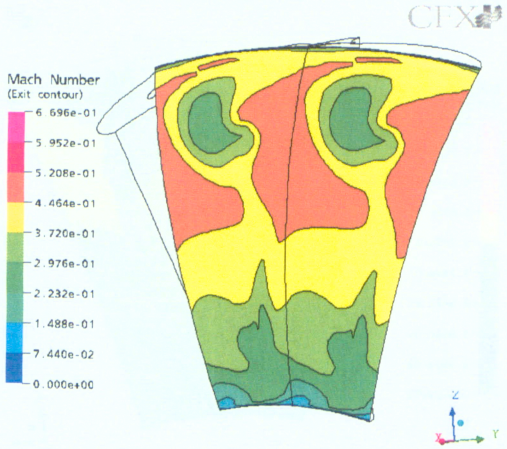

IGVV8

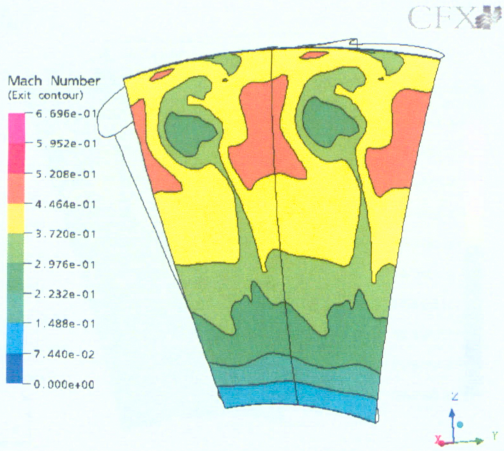

IGVV10

At 60 degree stagger:

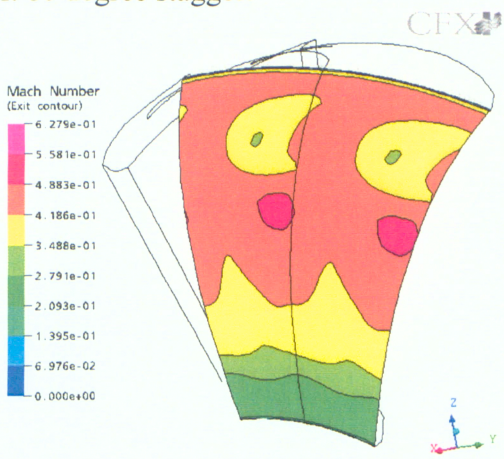

IGVV0

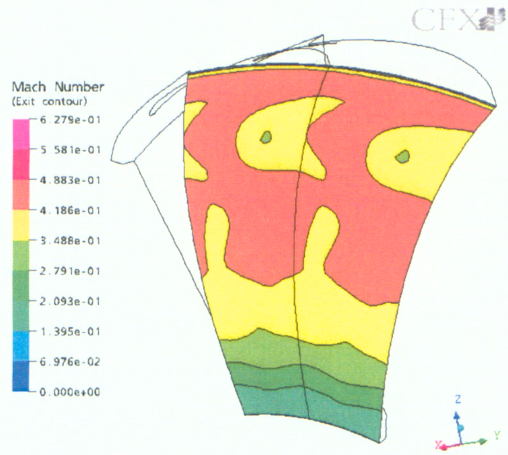

IGVV3

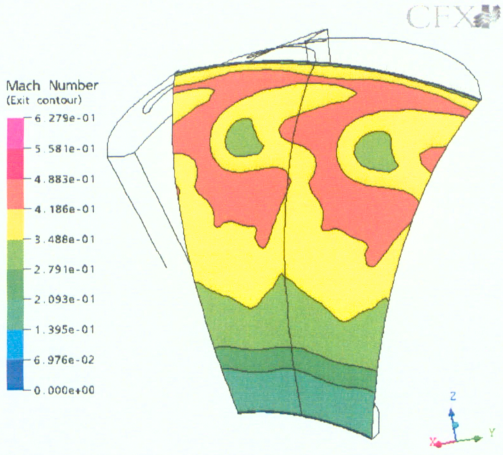

IGVV5

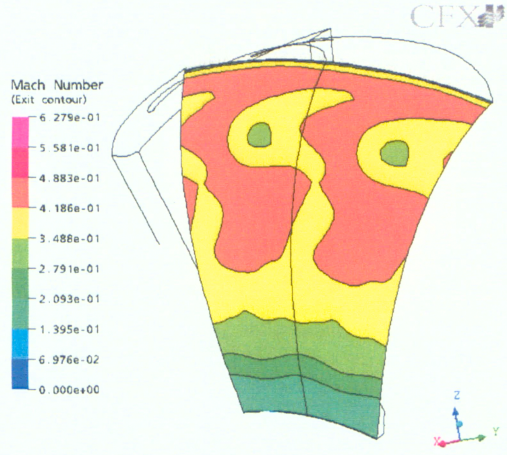

IGVV8

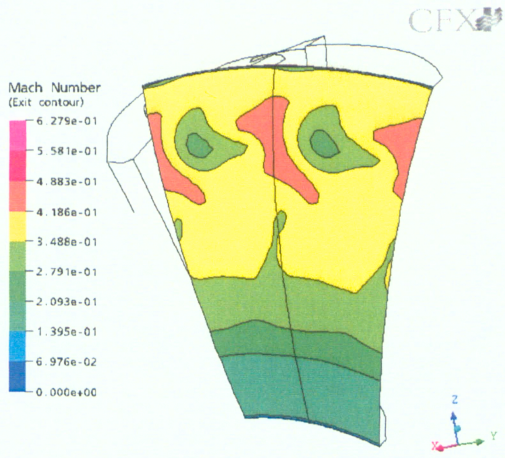

IGVV10